

Lighting up the Photon Wigner Distribution via Dilepton Productions

Yu Shi,^{1,2,*} Lin Chen,^{3,4,5,†} Shu-Yi Wei,^{1,‡} and Bo-Wen Xiao^{3,6,§}

¹*Key Laboratory of Particle Physics and Particle Irradiation (MOE),
Institute of frontier and interdisciplinary science,
Shandong University, Qingdao, Shandong 266237, China*

²*CPHT, CNRS, École polytechnique, Institut Polytechnique de Paris, 91120 Palaiseau, France*

³*School of Science and Engineering, The Chinese University of Hong Kong, Shenzhen, Guangdong, 518172, P.R. China*

⁴*University of Science and Technology of China, Hefei, Anhui, 230026, P.R.China*

⁵*Instituto Galego de Física de Altas Enerxías IGFAE,*

Universidade de Santiago de Compostela, E-15782 Galicia-Spain

⁶*Southern Center for Nuclear-Science Theory (SCNT), Institute of Modern Physics,
Chinese Academy of Sciences, Huizhou 516000, Guangdong Province, China*

We present a systematic investigation of lepton pair production through photon-photon fusion processes in heavy-ion collisions. It is demonstrated that the dilepton production at a given impact parameter (b_{\perp}) with a fixed transverse momentum imbalance (q_{\perp}) can be factorized into a unified formula in terms of the Wigner photon distribution of heavy nuclei. We show that this framework provides a comprehensive description of all the relevant data from RHIC to the LHC, with a strong evidence that the quasi-real photon can be radiated not only from the nucleus as a whole, standing for the coherent contribution, but also from the sub-structures inside the nucleus, representing the incoherent contribution. Further predictions are made for the anisotropies in the correlations between q_{\perp} , b_{\perp} , and the dilepton transverse momentum (P_{\perp}). This will help us to constrain the photon Wigner distribution which plays a crucial role to study the gluonic matter of nucleus at small- x through the diffractive photoproduction processes in heavy ion collision.

Introduction Dilepton production in photon-induced events measured in ultra-peripheral collisions (UPCs) has become a rich physics program at the Relativistic Heavy Ion Collider (RHIC) and the Large Hadron Collider (LHC). Due to a large photon flux surrounding the relativistic heavy nuclei, one can measure the dilepton production at an abundant rate and provide detailed information for this process at various transverse momentum (P_{\perp}), the transverse momentum imbalance (q_{\perp}), and the impact parameter (b_{\perp}). In recent years, abundant high-precision experimental data on dilepton production through photon-photon fusion process ($\gamma\gamma \rightarrow l^+l^-$) has been collected at RHIC [1–3] and the LHC [4–12]. A large number of diverse observables from the experimental measurement have been provided to understand and study its production mechanism. As it provides a clean environment to study the photon distributions from heavy nuclei, this process has attracted much attention which leads to a series of theoretical researches [13–57] and Monte-Carlo studies [58–62]. Additionally, this process improves our understanding of photo-nuclear interaction and the structure of the nucleus, and is important to explore new physics beyond the standard model [11, 63–68] and study QED properties under extreme conditions [40, 69–74].

Currently, different high-precision physical observables from RHIC and the LHC present a challenge to theo-

rists: to develop a unified factorized framework incorporating both impact parameter dependence and transverse momentum dependence, which can account for all experimental observables, such as dilepton anisotropies and q_{\perp} broadening. Based on previous studies[37–41], we derive a generalized factorization framework on dilepton production in terms of the photon fusion hard part and the photon Wigner distributions, which provide five-dimensional photon distribution within the nuclei. We will show that this framework not only reproduces the results from previous studies[37–39, 41], but also reveal a range of new anisotropic correlations among the vectors \vec{P}_{\perp} , \vec{q}_{\perp} , and \vec{b}_{\perp} . These anisotropies are useful for probing the properties of linearly polarized photons in heavy nuclei.

With a detailed analysis, we also find that the quasi-real photons not only can be emitted coherently from the nucleus as a whole but also incoherently from the substructures within the nucleus. Specifically, the incoherent contribution is one of the production mechanisms responsible for q_{\perp} broadening, and it predominantly contributes to events with neutron emissions in the large- q_{\perp} region. Thus, we provide a thorough description of existing experimental measurements from RHIC and LHC within this unified framework.

More recently, diffractive photo-production processes in heavy ion collisions, such as heavy quarkonium production, have been shown to provide a unique probe of gluon tomography in nuclei at small- x [75–87]. Because these processes also depend on the incoming photon Wigner distribution, the formalism derived in our paper will help solidify the theoretical foundation for these studies. In other words, a comparative study between

* yu.shi@polytechnique.edu

† lin.chen@usc.es

‡ shuyi@sdu.edu.cn

§ xiaobowen@cuhk.edu.cn

dilepton production through photon-photon fusion and diffractive photo-production will assist in building a rigorous framework to explore gluonic matter in cold nuclei during heavy ion collisions.

The generalized factorization Let us describe the generalized factorization for the dilepton production in the two-photon fusion process as follows

$$\gamma(k_1) + \gamma(k_2) \rightarrow l^+(p_1) + l^-(p_2). \quad (1)$$

In heavy-ion collisions, two high-energy nuclei, separated by a transverse distance b_\perp , emit a significant number of quasi-real photons with low virtuality. Two photons from different sources collide to produce a lepton pair with transverse momentum $p_{1\perp}$ and $p_{2\perp}$. The collision point is distanced at $b_{1\perp}$ and $b_{2\perp}$ from the two heavy nuclei, respectively. In both RHIC and the LHC experiments, measurements have shown that the transverse momentum of the final lepton is often much larger than the total momentum of the lepton pair, $\vec{q}_\perp = \vec{p}_{1\perp} + \vec{p}_{2\perp}$. Consequently, we can assume that the relative momentum of the lepton pair, $\vec{P}_\perp = (\vec{p}_{1\perp} - \vec{p}_{2\perp})/2$ with $P_\perp \gg q_\perp$, which is widely referred to as the back-to-back correlation limit. In this situation, one often needs to use the generalized equivalent photon approximation and the photon Wigner distribution to describe these quasi-real photons. The photon Wigner distribution, a quasi probability distribution function, includes the five-dimensional information of longitudinal momentum fraction, transverse momentum, and impart parameter of the photon, which is defined as [39, 88–95]

$$\Gamma^{ij}(x, \vec{k}_T, \vec{b}_\perp) = \int \frac{d^2\Delta_\perp}{(2\pi)^2} e^{i\Delta_\perp \cdot b_\perp} \Gamma^{ij}(x, \vec{k}_T, \vec{\Delta}_\perp), \quad (2)$$

and $\Gamma^{ij}(x, \vec{k}_T, \vec{\Delta}_\perp)$ represents the so-called Generalized Transverse Momentum Dependent (GTMD) photon distributions in the momentum space. It reads

$$\begin{aligned} \Gamma^{ij}(x, \vec{k}_T, \vec{\Delta}_\perp) &= \int \frac{d\xi^- d^2r_\perp}{(2\pi)^3} e^{ixP^+\xi^- - ik_T \cdot r_\perp} \\ &\times \langle A, -\frac{\Delta_\perp}{2} | F^{+i}(0, \frac{r_\perp}{2}) F^{+j}(\xi^-, -\frac{r_\perp}{2}) | \frac{\Delta_\perp}{2}, A \rangle, \end{aligned} \quad (3)$$

with the two dimensional polarization indices i for the incoming photon in the scattering amplitude and the polarization indices j for the photon in the conjugate amplitude. k_T represents the transverse momentum of the photon, and Δ_\perp corresponds to the Fourier transform of b_\perp . Meanwhile, x stands for the longitudinal momentum fractions of the photon per nucleon. Conventionally, the GTMD photon distributions can be parametrized into two parts: the unpolarized photon distribution $x f_\gamma(x, \vec{k}_T, \vec{\Delta}_\perp)$ and the linearly-polarized photon distribution $x h_\gamma(x, \vec{k}_T, \vec{\Delta}_\perp)$. It is defined as

$$\Gamma^{ij}(x, \vec{k}_T, \vec{\Delta}_\perp) = \frac{\delta^{ij}}{2} x f_\gamma(x, \vec{k}_T, \vec{\Delta}_\perp)$$

$$+ \left(\frac{k_+^i k_-^j}{\vec{k}_- \cdot \vec{k}_+} - \frac{\delta^{ij}}{2} \right) x h_\gamma(x, \vec{k}_T, \vec{\Delta}_\perp) \quad (4)$$

with $k_\pm = k_T \pm \Delta_\perp/2$. In the correlation limit assumption, the dilepton production from the two-photon fusion process can be separated into two parts: the Wigner distribution and the hard scattering part. Thus, the factorization formula reads as follows

$$\begin{aligned} \frac{d\sigma}{dy_1 dy_2 d^2q_\perp d^2P_\perp d^2b_\perp} &= \int \Gamma_{ij}(x_1, \vec{k}_{1T}, \vec{b}_{1\perp}) \otimes \\ &\Gamma_{kl}(x_2, \vec{k}_{2T}, \vec{b}_{2\perp}) \otimes \mathcal{H}^{ijkl}(\vec{P}_\perp). \end{aligned} \quad (5)$$

The two photon Wigner distributions, Γ_{ij} and Γ_{kl} , contain the photon distribution information with the momentum scales significantly less than P_\perp . The hard factor, \mathcal{H}^{ijkl} , represents the hard scale part and depends on the momentum imbalance of the lepton pair P_\perp and its angle ϕ_P . Since the lepton mass m_l is much smaller than P_\perp , we have neglected the lepton mass in the hard factor. The hard factor can be expressed as follows

$$\mathcal{H}^{ijkl}(\vec{P}_\perp) = \frac{\alpha_{\text{em}}^2}{\hat{s}^2} \left[O^{ijkl}(\vec{P}_\perp) - 4\Omega^{ijkl}(\vec{P}_\perp) \right], \quad (6)$$

with the projection hard parts O^{ijkl} and Ω^{ijkl} defined as

$$\begin{aligned} O^{ijkl}(\vec{P}_\perp) &= 2 \left(\frac{\hat{u}}{\hat{t}} + \frac{\hat{t}}{\hat{u}} \right) (\delta^{ij}\delta^{kl} - \delta^{ik}\delta^{jl} + \delta^{il}\delta^{jk}), \quad (7) \\ \Omega^{ijkl}(\vec{P}_\perp) &= 2\Pi^{ij}(\vec{P}_\perp)\Pi^{kl}(\vec{P}_\perp) \\ &\quad - (\delta^{il}\delta^{jk} + \delta^{ik}\delta^{jl} - \delta^{ij}\delta^{kl}), \end{aligned} \quad (8)$$

where \hat{s} , \hat{u} and \hat{t} are the Mandelstam variables and $\Pi^{ij}(\vec{P}_\perp) = 2\frac{P_\perp^i P_\perp^j}{P_\perp^2} - \delta^{ij}$. The first term O^{ijkl} is isotropic in terms of the angle ϕ_P as derived in Refs. [19, 39]. The second term, Ω^{ijkl} , can generate azimuthal asymmetries between two linearly polarized photons. Given an arbitrary two-dimensional unit vector \hat{n} , it is interesting to note the following tensor contractions: $\hat{n}_i \hat{n}_j \Pi^{ij} = \cos(2\Delta\phi)$ and $\hat{n}_i \hat{n}_j \hat{n}_k \hat{n}_l \Omega^{ijkl} = \cos(4\Delta\phi)$, where $\Delta\phi$ represents the azimuthal angle between \vec{P}_\perp and \hat{n} . Integrating over the angle of impact parameter ϕ_b , we find that the Ω^{ijkl} term projects the cross-section onto the $\cos(4\phi_P - 4\phi_q)$ harmonics, reproducing the result derived in Ref. [38]. Similarly, after integrating over q_\perp , one obtains the $\cos(4\phi_P - 4\phi_b)$ azimuthal asymmetry proposed in Ref. [41] from the Ω^{ijkl} tensor. In general, various azimuthal angle asymmetries can arise from inner products of the three vectors \vec{P}_\perp , \vec{q}_\perp , and \vec{b}_\perp .

As discussed in Ref. [39], it is vital to demonstrate that this dilepton production cross-section always remains positive definite although the photon Wigner distribution may become negative. Let us rewrite the photon GTMD distribution as

$$\Gamma^{ij}(x_1, \vec{k}_{1T}, \vec{\Delta}_\perp) = \frac{Z^2 \alpha_{\text{em}}}{\pi^2} k_{1\perp}^i k_{1\perp}^j \frac{F_A(k_1)}{k_1^2} \frac{F_A(k'_1)}{k_1'^2}, \quad (9)$$

where $F_A(k_1)$ is the elastic charge form factor, Z is charge number and m_p is the mass of proton with $k_1^2 = x_1^2 m_p^2 + k_{1\perp}^2$ and $k_1'^2 = x_1^2 m_p^2 + k_{1\perp}'^2$. As detailed in the supplemental material, one finds

$$d\sigma \geq \left(\frac{Z^2}{\pi^2}\right)^2 \frac{8\alpha_{\text{em}}^4}{(2\pi)^2 \hat{s}^2} (G^{12} + G^{21})(G^{12*} + G^{21*}), \quad (10)$$

where $G^{ik} \equiv \int d^2k_{1\perp} e^{ik_{1\perp} \cdot b_\perp} F_A(k_1) F_A(k_2) |k_{1\perp}| |k_{2\perp}| \hat{l}_1^i \hat{l}_2^k$. The \hat{l}_i here refers to a unit vector, pointing the direction with the angle $\phi_{l_i} = \phi_{k_{i\perp}} - \phi_P$. Thus, it is clear that the cross-section is ensured to be positive definite.

Phenomenology Let us employ the unified factorization formalism to calculate various relevant observables, with a comprehensive phenomenological study available in the supplemental material.

First, the cross-section contains abundant angular correlation between the impact parameter and the transverse momentum of the final particles, and it can be decomposed as follows

$$\begin{aligned} \sigma = & \sigma_0 + \sigma_{2qb} \cos(2\phi_q - 2\phi_b) + \sigma_{4qb} \cos(4\phi_q - 4\phi_b) \\ & + \sigma_{4qP} \cos(4\phi_q - 4\phi_P) + \sigma_{4bP} \cos(4\phi_b - 4\phi_P) \\ & + \sigma_{qbP} \cos(2\phi_q + 2\phi_b - 4\phi_P) + \dots, \end{aligned} \quad (11)$$

where the coefficients $\sigma_{2qb}, \sigma_{4qb}, \dots$ encode various information of the photon flux. As shown in Refs. [37–41, 43–45, 53, 55], the linearly polarized photons can generate a range of angular correlations either between P_\perp and q_\perp (including $\Delta\phi$ or α distributions at fixed b_\perp), or between P_\perp and b_\perp . From the unified framework, one sees that there are a series of non-trivial angular correlations among q_\perp , b_\perp , and P_\perp . We find that these anisotropies can be divided into two categories. The first category, which does not depend on P_\perp , arises from the contraction between the O^{ijkl} term of hard factor and the photon Wigner distributions. It leads to two sizable anisotropies, $2\langle \cos(2\phi_b - 2\phi_q) \rangle$ and $2\langle \cos(4\phi_b - 4\phi_q) \rangle$. The other category, which involves the $\cos(4\phi_P)$ correlation, is due to the contraction between the Ω^{ijkl} term and the photon Wigner distributions. We can reproduce the two anisotropies, $2\langle \cos(4\phi_P - 4\phi_q) \rangle$ and $2\langle \cos(4\phi_P - 4\phi_b) \rangle$, as proposed earlier in Refs. [37, 38, 41]. Also, we find that there are additional novel angular correlations, such as $2\langle \cos(2\phi_q + 2\phi_b - 4\phi_P) \rangle$, $2\langle \cos(6\phi_q - 2\phi_b - 4\phi_P) \rangle$ and $2\langle \cos(6\phi_b - 2\phi_q - 4\phi_P) \rangle$, etc. It is interesting to note that the impact parameter vector \vec{b}_\perp can be determined through the reaction plane of the hadronic events in peripheral collisions. Therefore, combined with the additional information provided by the momentum anisotropy of the produced hadrons in the same event, it is possible to measure all the aforementioned dilepton angular correlations among q_\perp , P_\perp , and b_\perp in peripheral collisions at RHIC and the LHC.

To provide a complete description of the most up-to-date data, we also need to include the incoherent contributions from the interior of the colliding nuclei. When the transverse momentum of incoming photons is less

than $1/R_A$ with R_A the nuclear radius, one can view the nucleus as a coherent charge source of photons. While incoming photons emerge incoherently from the interior of the heavy nuclei, they often carry much larger transverse momentum as they resolve the nucleus' internal sub-structure. This scenario is often accompanied by the dissociation of these nuclei. The STAR, CMS and ATLAS Collaborations have recently published a substantial amount of data related to neutron emissions and nuclear break-ups in UPCs [3, 6, 7, 10]. In the following, we examine the role of incoherent contributions in events involving neutron emissions.

In the $0n0n$ scenario in which no neutron is detected, the heavy nucleus remains intact. The primary contribution comes from the coherent photons. As substantiated in previous studies [32, 39, 55], the large transverse momentum imbalance of the lepton pair induced by the final-state soft multi-photon radiation can be effectively addressed through the Sudakov resummation. The detailed implementation is provided in the supplemental material. On the other hand, for the $XnXn$ cases where neutron emissions are observed, the heavy nucleus is considered disintegrated, indicating the presence of not only the final-state soft multi-photon radiation but also incoherent interactions in these events. Therefore, taking into account photons come from different sources, we modified the GTMD photon distribution $\Gamma^{ij}(x, k_T, \Delta)$ as follows

$$\begin{aligned} \Gamma^{ij}(x, \vec{k}_T, \vec{\Delta}_\perp) = & \Gamma_A^{ij}(x, \vec{k}_T, \vec{\Delta}_\perp) + \Gamma_p^{ij}(x, \vec{k}_T, \vec{\Delta}_\perp) \\ & + \Gamma_q^{ij}(x, \vec{k}_T, \vec{\Delta}_\perp). \end{aligned} \quad (12)$$

The first term $\Gamma_A^{ij}(x, \vec{k}_T, \vec{\Delta}_\perp)$ represents the coherent contribution from the heavy nucleus, acting as a whole, as the photon source. The second term $\Gamma_p^{ij}(x, \vec{k}_T, \vec{\Delta}_\perp)$ signifies that the proton inside the nucleus plays the role of the individual photon source, which is given by

$$\Gamma_p^{ij}(x, \vec{k}_T, \vec{\Delta}_\perp) = \frac{Z\alpha_{\text{em}}}{\pi^2} k_\perp^i k_\perp^j \frac{F_p(k)}{k^2} \frac{F_p(k')}{k'^2}, \quad (13)$$

where $F_p(k)$ stands for the proton charge form factor. The last term corresponds to the incoherent contribution originated from quarks inside nucleons. By treating quarks as point-like particles, then the corresponding GTMD photon distribution $\Gamma_q^{ij}(x, \vec{k}_T, \vec{\Delta}_\perp)$ reads

$$\Gamma_q^{ij}(x, \vec{k}_T, \vec{\Delta}_\perp) = \alpha_{\text{em}} \frac{\sum_q e_q^2}{\pi^2} k_\perp^i k_\perp^j \frac{1}{k^2} \frac{1}{k'^2}, \quad (14)$$

where e_q is the quark charge number. In the experimental measurements, the maximum value of transverse momentum imbalance is approximately 1.2 GeV, which is already much larger than the typical confinement scale. Thus, at a scale around 1 GeV, dilepton production is capable of resolving quarks within the proton, although fluctuations inside the nucleon remain relatively insignificant. Consequently, for the sake of simplifying the calculation, we utilize the valence quark model to outline

the quark distribution within both the proton and the neutron. We assume that these three quarks, two up quarks and one down quark, share the same momentum within the proton. Similarly, two down quarks and one up quark share the same momentum within the neutron. The above approximation can be improved by following a recent study of the photon parton distribution in the proton [96, 97], where a rigorous connection to the proton structure functions played an important role. We expect a similar treatment can be made for the above incoherent contribution to the photon Wigner distribution. We will leave this issue for a later publication.

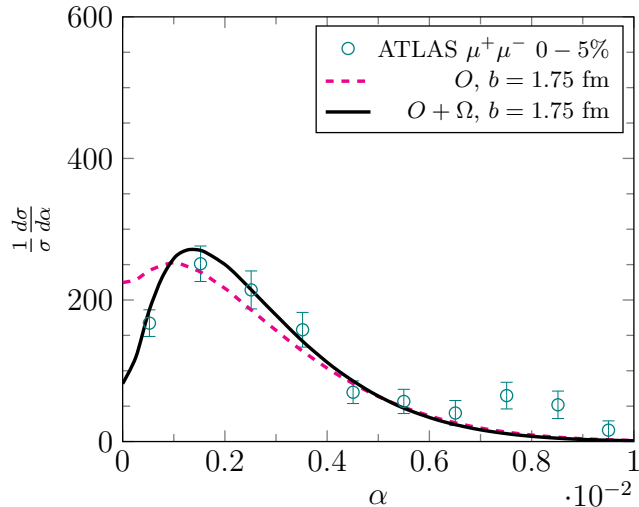


FIG. 1. Comparison the numerical results with the ATLAS measurement of the dimuon pair acoplanarity α distribution in central collisions [9].

Comparing with data In our numerical calculation, we follow the STARlight [58] and use the nucleus form factor [98]

$$F_A(k) = \frac{3}{(kR_A)^3} \frac{[\sin(kR_A) - kR_A \cos(kR_A)]}{1 + a^2 k^2}, \quad (15)$$

with $a = 0.71$ fm, R_A nucleus radius and A the number of nucleons in the nucleus. We set $R_A = 6.6$ fm for the lead nucleus. For the proton, we employ the dipole form factor [99, 100]

$$F_p(k) = \frac{1}{[(k^2/0.71 \text{ GeV}^2) + 1]^2}. \quad (16)$$

As depicted in Fig. 1, we compare our results with the α distribution data from the ATLAS Collaboration [9] in the 0 – 5% centrality interval. The acoplanarity α is defined by $\alpha = 1 - \Delta\phi/\pi$, where $\Delta\phi$ denotes the angular difference between two leptons. The magenta dashed line represents the computation derived from the first term O^{ijkl} of the hard factor, whereas the black solid line indicates the calculation resulting from both the first term O^{ijkl} and the second term $\Omega^{ijkl}(\vec{P}_\perp)$. In the small α region, there is a notable gap between the result computed

from the first term O^{ijkl} of the hard factor and the experimental data. However, after including the second term $\Omega^{ijkl}(\vec{P}_\perp)$, our calculation can reproduce the dip shape observed in the experiment and perfectly aligns with the ATLAS experimental data, thereby highlighting the importance of the $\Omega^{ijkl}(\vec{P}_\perp)$ term in describing the dip in the extremely small α region. Similar numerical results can also be found in the calculations in Refs. [35, 37, 38, 48, 50, 55]. As α increases, we find that the contribution of the $\Omega^{ijkl}(\vec{P}_\perp)$ term tends to diminish, and the O^{ijkl} term takes the dominant contribution.

We compare our numerical calculations for the α distribution involving neutron emissions with the CMS $XnXn$ and ATLAS $MnMn$ data [7, 10] in Fig. 2. In the CMS experiment, Xn represents the emission of two or more neutrons, whereas Mn denotes the emission of one or more neutrons in the ATLAS experiment. The magenta dash-dotted line stands for the coherent calculation without the Sudakov effect, and the blue dashed line corresponds to the coherent calculation with the Sudakov effect. In addition, the orange dotted line represents the sum of the coherent and incoherent contribution without the Sudakov effect. At last, the solid line includes both incoherent contribution and the Sudakov effect.

All four calculations agree in the small- α region, meaning that the coherent term originating from the nucleus acting as the photon source is the dominant contribution, and the incoherent contribution and Sudakov effect are negligible in this region. In the large- α region, both the Sudakov effect and the incoherent contribution are important mechanisms leading to the final q_\perp broadening. However, neither of these mechanisms alone can accurately describe the data with neutron emissions. When both mechanisms are considered, we can obtain the enhanced broadening effect and find good agreements with the CMS and ATLAS data. This implies that the final q_\perp broadening in the large- α region receive contributions from both the Sudakov effect and the incoherent contribution. In the small- α region, the corresponding transverse momentum imbalance, $q_\perp \sim \pi\alpha P_\perp$, is less than 30 MeV. As a result, dileptons cannot penetrate or “see” the inner structure of heavy nuclei, allowing the heavy nucleus to be perceived as a whole entity radiating photons. However, as α increases, q_\perp can rise up to 1 ~ 3 GeV. This enables the dilepton to resolve the inner structure of heavy nuclei, such as protons and quarks. Consequently, quarks and protons begin to act as incoherent photon sources in the large α region.

Conclusion In this paper, we present a unified factorized framework, involving the photon Wigner distribution, to study the lepton pair production via the photon fusion process in heavy-ion collisions. Furthermore, we show that various correlations exist between lepton’s transverse momentum P_\perp , the imbalance of transverse momentum q_\perp , and the impact parameter b_\perp . Future experimental studies can explore these anisotropies in heavy-ion collisions at RHIC and the LHC. Additionally, our study shows that the photon source is not solely from

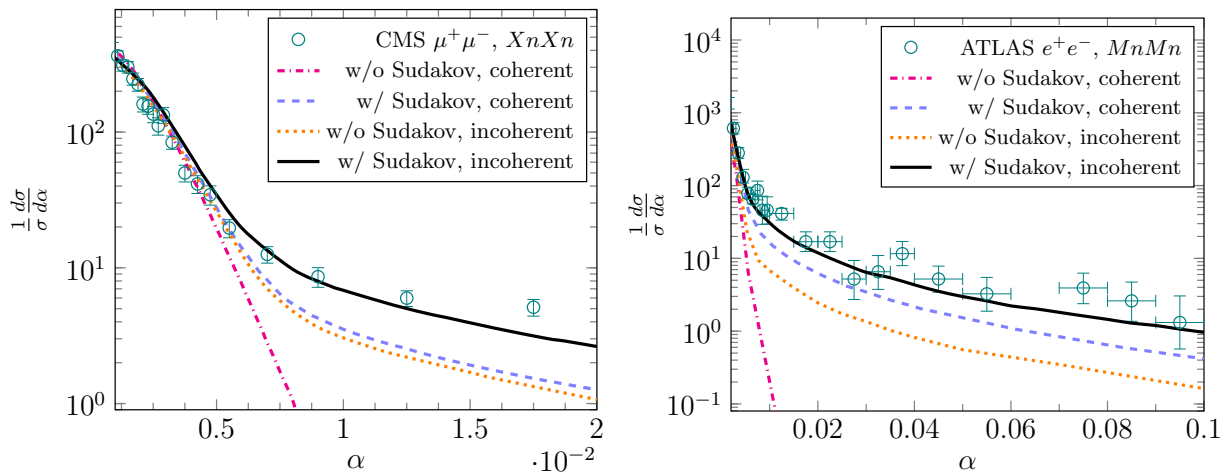


FIG. 2. Comparisons of the numerical results with the CMS $XnXn$ data [7] and the ATLAS $MnMn$ data [10].

the heavy nucleus as a whole but also from the protons inside the nucleus and the substructure of the nucleons (the quarks). Considering events accompanied by neutron emissions measured at the LHC, we show that the incoherent contributions are significant in the large- α region. Our unified factorized formula has successfully described a wide range of relevant data from the STAR, CMS, and ATLAS Collaborations. Finally, this unified factorization formula, developed in this study, can offer novel perspectives for exploring the factorization and

production mechanisms of other processes in UPCs.

Acknowledgments We thank Feng Yuan, Jian Zhou, Cheng Zhang, Ya-Jin Zhou and Shi Pu for useful inputs and discussions. This work is partly supported by the CUHK-Shenzhen under grant No. UDF01001859. Y. Shi is supported by the China Postdoctoral Science Foundation under Grant No. 2022M720082. S.Y. Wei is supported by the Shandong Province Natural Science Foundation under grant No. 2023HWYQ-011 and the Taishan fellowship of Shandong Province for junior scientists.

-
- [1] J. Adams *et al.* [STAR], Phys. Rev. C **70**, 031902 (2004) [arXiv:nucl-ex/0404012 [nucl-ex]].
- [2] J. Adam *et al.* [STAR], Phys. Rev. Lett. **121**, no.13, 132301 (2018) [arXiv:1806.02295 [hep-ex]].
- [3] J. Adam *et al.* [STAR], Phys. Rev. Lett. **127**, no.5, 052302 (2021) [arXiv:1910.12400 [nucl-ex]].
- [4] [ATLAS], ATLAS-CONF-2016-025.
- [5] M. Aaboud *et al.* [ATLAS], Phys. Rev. Lett. **121**, no.21, 212301 (2018) [arXiv:1806.08708 [nucl-ex]].
- [6] G. Aad *et al.* [ATLAS], Phys. Rev. C **104**, 024906 (2021) [arXiv:2011.12211 [nucl-ex]].
- [7] A. M. Sirunyan *et al.* [CMS], Phys. Rev. Lett. **127**, no.12, 122001 (2021) [arXiv:2011.05239 [hep-ex]].
- [8] S. Acharya *et al.* [ALICE], JHEP **06**, 024 (2023) [arXiv:2204.11732 [nucl-ex]].
- [9] G. Aad *et al.* [ATLAS], Phys. Rev. C **107**, no.5, 054907 (2023) [arXiv:2206.12594 [nucl-ex]].
- [10] G. Aad *et al.* [ATLAS], JHEP **2306**, 182 (2023) [arXiv:2207.12781 [nucl-ex]].
- [11] G. Aad *et al.* [ATLAS], Phys. Rev. Lett. **131**, no.15, 151802 (2023) [arXiv:2204.13478 [hep-ex]].
- [12] A. Tumasyan *et al.* [CMS], Phys. Rev. Lett. **131**, 151803 (2023) [arXiv:2206.05192 [nucl-ex]].
- [13] S. J. Brodsky, T. Kinoshita and H. Terazawa, Phys. Rev. D **4**, 1532-1557 (1971).
- [14] H. Terazawa, Rev. Mod. Phys. **45**, 615-662 (1973).
- [15] V. M. Budnev, I. F. Ginzburg, G. V. Meledin and V. G. Serbo, Phys. Rept. **15**, 181-281 (1975).
- [16] C. A. Bertulani and G. Baur, Phys. Rept. **163**, 299 (1988).
- [17] R. N. Cahn and J. D. Jackson, Phys. Rev. D **42**, 3690-3695 (1990).
- [18] C. Bottcher, M. R. Strayer and M. J. Rhoades-Brown, Phys. Rev. A **44**, 4769-4770 (1991).
- [19] M. Vidovic, M. Greiner, C. Best and G. Soff, Phys. Rev. C **47**, 2308-2319 (1993).
- [20] K. Hencken, D. Trautmann and G. Baur, Phys. Rev. A **51**, 1874-1882 (1995) [arXiv:nucl-th/9410014 [nucl-th]].
- [21] F. Krauss, M. Greiner and G. Soff, Prog. Part. Nucl. Phys. **39**, 503-564 (1997).
- [22] M. C. Guclu, J. Li, A. S. Umar, D. J. Ernst and M. R. Strayer, Annals Phys. **272**, 7-48 (1999).
- [23] G. Baur, K. Hencken, D. Trautmann, S. Sadovskiy and Y. Kharlov, Phys. Rept. **364**, 359-450 (2002) [arXiv:hep-ph/0112211 [hep-ph]].
- [24] A. J. Baltz, S. R. Klein and J. Nystrand, Phys. Rev. Lett. **89**, 012301 (2002) [arXiv:nucl-th/0205031 [nucl-th]].
- [25] G. Baur, K. Hencken, A. Aste, D. Trautmann and S. R. Klein, Nucl. Phys. A **729**, 787-808 (2003) [arXiv:nucl-th/0307031 [nucl-th]].
- [26] K. Hencken, G. Baur and D. Trautmann, Phys. Rev. C **69**, 054902 (2004) [arXiv:nucl-th/0402061 [nucl-th]].
- [27] C. A. Bertulani, S. R. Klein and J. Nystrand, Ann. Rev. Nucl. Part. Sci. **55**, 271-310 (2005) [arXiv:nucl-ex/0502005 [nucl-ex]].

- [28] G. Baur, K. Hencken and D. Trautmann, Phys. Rept. **453**, 1-27 (2007) [arXiv:0706.0654 [nucl-th]].
- [29] A. J. Baltz, G. Baur, D. d'Enterria, L. Frankfurt, F. Gelis, V. Guzey, K. Hencken, Y. Kharlov, M. Klasen and S. R. Klein, *et al.* Phys. Rept. **458**, 1-171 (2008) [arXiv:0706.3356 [nucl-ex]].
- [30] A. J. Baltz, Y. Gorbunov, S. R. Klein and J. Nystrand, Phys. Rev. C **80**, 044902 (2009) [arXiv:0907.1214 [nucl-ex]].
- [31] S. R. Klein, Phys. Rev. C **97**, no.5, 054903 (2018) [arXiv:1801.04320 [nucl-th]].
- [32] S. Klein, A. H. Mueller, B. W. Xiao and F. Yuan, Phys. Rev. Lett. **122**, no.13, 132301 (2019) [arXiv:1811.05519 [hep-ph]].
- [33] M. Klusek-Gawenda, R. Rapp, W. Schäfer and A. Szczurek, Phys. Lett. B **790**, 339-344 (2019) [arXiv:1809.07049 [nucl-th]].
- [34] M. I. Vysotskii and E. Zhemchugov, Phys. Usp. **62**, no.9, 910-919 (2019) [arXiv:1806.07238 [hep-ph]].
- [35] W. Zha, J. D. Brandenburg, Z. Tang and Z. Xu, Phys. Lett. B **800**, 135089 (2020) [arXiv:1812.02820 [nucl-th]].
- [36] C. Azevedo, V. P. Gonçalves and B. D. Moreira, Eur. Phys. J. C **79**, no.5, 432 (2019) [arXiv:1902.00268 [hep-ph]].
- [37] C. Li, J. Zhou and Y. J. Zhou, Phys. Lett. B **795**, 576-580 (2019) [arXiv:1903.10084 [hep-ph]].
- [38] C. Li, J. Zhou and Y. J. Zhou, Phys. Rev. D **101**, no.3, 034015 (2020) [arXiv:1911.00237 [hep-ph]].
- [39] S. Klein, A. H. Mueller, B. W. Xiao and F. Yuan, Phys. Rev. D **102**, no.9, 094013 (2020) [arXiv:2003.02947 [hep-ph]].
- [40] S. Klein and P. Steinberg, Ann. Rev. Nucl. Part. Sci. **70**, 323-354 (2020) [arXiv:2005.01872 [nucl-ex]].
- [41] B. W. Xiao, F. Yuan and J. Zhou, Phys. Rev. Lett. **125**, no.23, 232301 (2020) [arXiv:2003.06352 [hep-ph]].
- [42] S. Karadağ and M. C. Güçlü, Phys. Rev. C **102**, no.1, 014904 (2020) [arXiv:1911.08507 [hep-ph]].
- [43] M. Klusek-Gawenda, W. Schäfer and A. Szczurek, Phys. Lett. B **814**, 136114 (2021) [arXiv:2012.11973 [hep-ph]].
- [44] J. D. Brandenburg, W. Li, L. Ruan, Z. Tang, Z. Xu, S. Yang and W. Zha, [arXiv:2006.07365 [hep-ph]].
- [45] W. Zha, J. D. Brandenburg, L. Ruan, Z. Tang and Z. Xu, Phys. Rev. D **103**, no.3, 033007 (2021) [arXiv:2006.12099 [hep-ph]].
- [46] Y. Hatta, B. W. Xiao, F. Yuan and J. Zhou, Phys. Rev. D **104**, no.5, 054037 (2021) [arXiv:2106.05307 [hep-ph]].
- [47] W. Zha and Z. Tang, JHEP **08**, 083 (2021) [arXiv:2103.04605 [hep-ph]].
- [48] R. j. Wang, S. Pu and Q. Wang, Phys. Rev. D **104**, no.5, 056011 (2021) [arXiv:2106.05462 [hep-ph]].
- [49] X. Wang, J. D. Brandenburg, L. Ruan, F. Shao, Z. Xu, C. Yang and W. Zha, Phys. Rev. C **107**, no.4, 044906 (2023) [arXiv:2207.05595 [nucl-th]].
- [50] R. j. Wang, S. Lin, S. Pu, Y. f. Zhang and Q. Wang, Phys. Rev. D **106**, no.3, 034025 (2022) [arXiv:2204.02761 [hep-ph]].
- [51] J. D. Brandenburg, J. Seger, Z. Xu and W. Zha, Rept. Prog. Phys. **86**, no.8, 083901 (2023) [arXiv:2208.14943 [hep-ph]].
- [52] S. Lin, R. J. Wang, J. F. Wang, H. J. Xu, S. Pu and Q. Wang, Phys. Rev. D **107**, no.5, 054004 (2023) [arXiv:2210.05106 [hep-ph]].
- [53] D. Y. Shao, C. Zhang, J. Zhou and Y. J. Zhou, Phys. Rev. D **107**, no.3, 036020 (2023) [arXiv:2212.05775 [hep-ph]].
- [54] J. Luo, X. Li, Z. Tang, X. Wu and W. Zha, Phys. Rev. C **108**, no.5, 054906 (2023) [arXiv:2308.03070 [hep-ph]].
- [55] D. Y. Shao, C. Zhang, J. Zhou and Y. j. Zhou, Phys. Rev. D **108**, no.11, 116015 (2023) [arXiv:2306.02337 [hep-ph]].
- [56] J. P. Dai and S. Zhao, Phys. Rev. D **109**, no.5, 054022 (2024) [arXiv:2401.04681 [hep-ph]].
- [57] C. Zhang, L. M. Zhang and D. Y. Shao, [arXiv:2406.05618 [hep-ph]].
- [58] S. R. Klein, J. Nystrand, J. Seger, Y. Gorbunov and J. Butterworth, Comput. Phys. Commun. **212**, 258-268 (2017) [arXiv:1607.03838 [hep-ph]].
- [59] L. A. Harland-Lang, V. A. Khoze and M. G. Ryskin, Eur. Phys. J. C **79**, no.1, 39 (2019) [arXiv:1810.06567 [hep-ph]].
- [60] N. Burmasov, E. Kryshen, P. Buehler and R. Lavicka, Comput. Phys. Commun. **277**, 108388 (2022) [arXiv:2111.11383 [hep-ph]].
- [61] H. S. Shao and D. d'Enterria, JHEP **09**, 248 (2022) [arXiv:2207.03012 [hep-ph]].
- [62] L. A. Harland-Lang, Phys. Rev. D **107**, no.9, 093004 (2023) [arXiv:2303.04826 [hep-ph]].
- [63] J. Abdallah *et al.* [DELPHI], Eur. Phys. J. C **35**, 159-170 (2004) [arXiv:hep-ex/0406010 [hep-ex]].
- [64] S. Knapen, T. Lin, H. K. Lou and T. Melia, Phys. Rev. Lett. **118**, no.17, 171801 (2017) [arXiv:1607.06083 [hep-ph]].
- [65] A. M. Sirunyan *et al.* [CMS], Phys. Lett. B **797**, 134826 (2019) [arXiv:1810.04602 [hep-ex]].
- [66] J. Ellis, N. E. Mavromatos and T. You, Phys. Rev. Lett. **118**, no.26, 261802 (2017) [arXiv:1703.08450 [hep-ph]].
- [67] I. Xu, N. Lewis, X. Wang, J. D. Brandenburg and L. Ruan, [arXiv:2211.02132 [hep-ex]].
- [68] D. Y. Shao, B. Yan, S. R. Yuan and C. Zhang, [arXiv:2310.14153 [hep-ph]].
- [69] G. Baur, K. Hencken and D. Trautmann, J. Phys. G **24**, 1657-1692 (1998) [arXiv:hep-ph/9804348 [hep-ph]].
- [70] A. J. Baltz and M. Strikman, Phys. Rev. D **57**, 548-549 (1998) [arXiv:hep-ph/9705220 [hep-ph]].
- [71] P. A. Steinberg [ALICE, ATLAS, CMS, LHCb and STAR], Nucl. Phys. A **1005**, 122007 (2021)
- [72] K. Hattori, H. Taya and S. Yoshida, JHEP **01**, 093 (2021) [arXiv:2010.13492 [hep-ph]].
- [73] P. Copinger and S. Pu, Int. J. Mod. Phys. A **35**, no.28, 2030015 (2020) [arXiv:2008.03635 [hep-ph]].
- [74] J. D. Brandenburg, W. Zha and Z. Xu, Eur. Phys. J. A **57**, no.10, 299 (2021) [arXiv:2103.16623 [hep-ph]].
- [75] S. R. Klein and H. Mäntysaari, Nature Rev. Phys. **1**, no.11, 662-674 (2019) [arXiv:1910.10858 [hep-ex]].
- [76] H. Mäntysaari, Rept. Prog. Phys. **83**, no.8, 082201 (2020) [arXiv:2001.10705 [hep-ph]].
- [77] H. Mäntysaari and R. Venugopalan, Phys. Lett. B **781**, 664-671 (2018) [arXiv:1712.02508 [nucl-th]].
- [78] A. Morreale and F. Salazar, Universe **7**, no.8, 312 (2021) [arXiv:2108.08254 [hep-ph]].
- [79] H. Mäntysaari, F. Salazar, B. Schenke, C. Shen and W. Zhao, Phys. Rev. C **109**, no.2, 024908 (2024) [arXiv:2310.15300 [nucl-th]].
- [80] H. Mäntysaari, F. Salazar and B. Schenke, [arXiv:2312.04194 [hep-ph]].
- [81] Y. V. Kovchegov, H. Sun and Z. Tu, [arXiv:2311.12208 [hep-ph]].
- [82] J. Cepila, J. G. Contreras, M. Matas and A. Ridzikova,

- [arXiv:2312.11320 [hep-ph]].
- [83] S. Acharya *et al.* [ALICE], Eur. Phys. J. C **81**, no.8, 712 (2021) [arXiv:2101.04577 [nucl-ex]].
- [84] A. Tumasyan *et al.* [CMS], Phys. Rev. Lett. **131**, no.26, 262301 (2023) [arXiv:2303.16984 [nucl-ex]].
- [85] R. Aaij *et al.* [LHCb], JHEP **06**, 146 (2023) [arXiv:2206.08221 [hep-ex]].
- [86] S. Acharya *et al.* [ALICE], JHEP **10**, 119 (2023) [arXiv:2305.19060 [nucl-ex]].
- [87] [STAR], [arXiv:2311.13637 [nucl-ex]].
- [88] C. F. von Weizsacker, Z. Phys. **88**, 612-625 (1934).
- [89] E. J. Williams, Phys. Rev. **45**, 729-730 (1934).
- [90] X. D. Ji, Phys. Rev. Lett. **78**, 610-613 (1997) [arXiv:hep-ph/9603249 [hep-ph]].
- [91] A. V. Belitsky and D. Mueller, Phys. Lett. B **486**, 369-377 (2000) [arXiv:hep-ph/0005028 [hep-ph]].
- [92] M. Diehl, Eur. Phys. J. C **19**, 485-492 (2001) [arXiv:hep-ph/0101335 [hep-ph]].
- [93] X. d. Ji, Phys. Rev. Lett. **91**, 062001 (2003) [arXiv:hep-ph/0304037 [hep-ph]].
- [94] A. V. Belitsky, X. d. Ji and F. Yuan, Phys. Rev. D **69**, 074014 (2004) [arXiv:hep-ph/0307383 [hep-ph]].
- [95] Y. Hatta, B. W. Xiao and F. Yuan, Phys. Rev. Lett. **116**, no.20, 202301 (2016) [arXiv:1601.01585 [hep-ph]].
- [96] A. Manohar, P. Nason, G. P. Salam and G. Zanderighi, Phys. Rev. Lett. **117**, no.24, 242002 (2016) [arXiv:1607.04266 [hep-ph]].
- [97] A. V. Manohar, P. Nason, G. P. Salam and G. Zanderighi, JHEP **12**, 046 (2017) [arXiv:1708.01256 [hep-ph]].
- [98] K. T. R. Davies and J. R. Nix, Phys. Rev. C **14**, 1977-1994 (1976)
- [99] L. Andivahis, P. E. Bosted, A. Lung, L. M. Stuart, J. Alster, R. G. Arnold, C. C. Chang, F. S. Dietrich, W. R. Dodge and R. Gearhart, *et al.* Phys. Rev. D **50**, 5491-5517 (1994)
- [100] S. R. Klein and J. Nystrand, Phys. Rev. Lett. **92**, 142003 (2004) [arXiv:hep-ph/0311164 [hep-ph]].

SUPPLEMENTAL MATERIAL

CONTENTS

References	5
1. The Generalized Factorization formalism	7
2. Phenomenological Studies	11
a. Anisotropies	11
b. The Sudakov Effect	13
c. Dilepton Events with Neutrons Emission	14
d. The Incoherent Contribution to the Photon Distribution	16
3. Comparisons with the RHIC and LHC data	18
a. Acoplanarity and Transverse Momentum Broadening	18
b. The Neutron Emission effect in the Small α Region	20
c. Enhancements from the Incoherent Contributions in the Large α Region	22

We provide additional details in the supplemental material. In Sec. 1, the generalized factorization framework for the dilepton production via the photon-photon fusion process in ultra-peripheral heavy-ion collisions is presented. Sec. 2 discusses several topics concerning the phenomenological studies. In Sec. 3, we present additional numerical results compared with the experimental data.

1. The Generalized Factorization formalism

The left figure in Fig. 3 shows the cartoon of the dilepton production from electromagnetic interactions in heavy-ion collisions: two quasi-real photons, each radiated from one of the two fast-moving nuclei at a relative distance b_{\perp} , undergo fusion to generate a pair of leptons. These leptons are almost back-to-back, each with transverse momentum $p_{1\perp}$ and $p_{2\perp}$, and are produced at the rapidity y_1 and y_2 , respectively. The collision point, where these leptons are produced, is situated at distances $b_{1\perp}$ and $b_{2\perp}$ from the two heavy nuclei.

In the following calculations, we assume that the relative transverse momentum of the lepton pair $\vec{P}_{\perp} = (\vec{p}_{1\perp} - \vec{p}_{2\perp})/2 \sim p_{1\perp} \sim p_{2\perp}$ is much large than the total transverse momentum of lepton pair $\vec{q}_{\perp} = \vec{p}_{1\perp} + \vec{p}_{2\perp}$. Thus, we can use the relative transverse momentum of the lepton pair P_{\perp} as the largest scale to factorize the process into two different parts, the hard part and the photon distribution part. The hard part corresponds to the hard interaction of lepton pair production, which depends on the hard momentum P_{\perp} and its azimuthal angle ϕ_P . The photon distributions involve soft momentum scales, which are of the order of q_{\perp} much less than P_{\perp} .

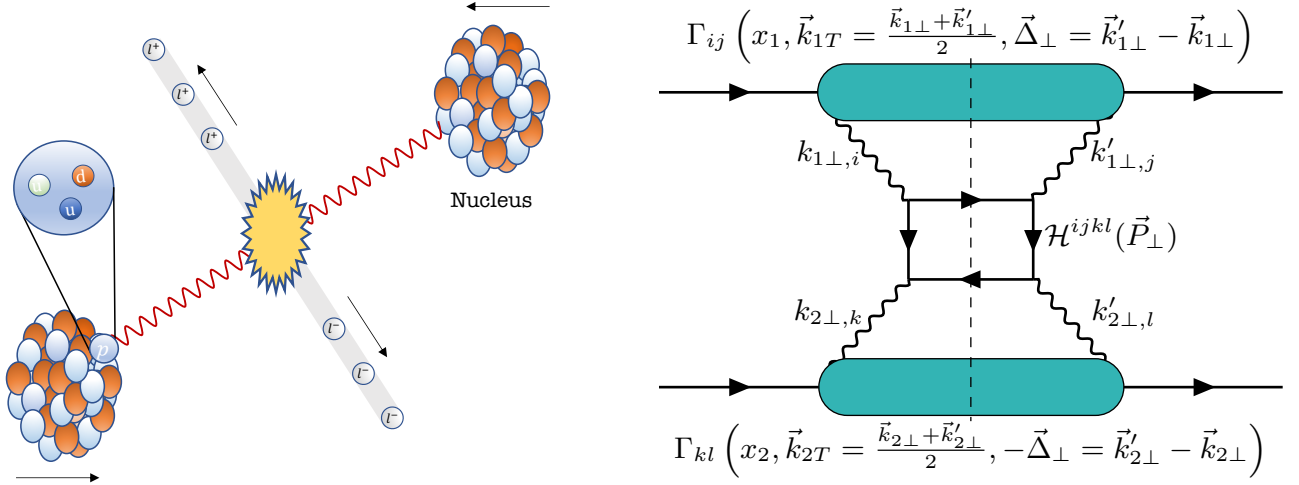


FIG. 3. Left: The cartoon depiction of the lepton pair production from the photon-photon fusion process in heavy-ion collisions. Right: The Feynman diagram illustrating the generalized TMD factorization for the $\gamma(k_1) + \gamma(k_2) \rightarrow l^+(p_1) + l^-(p_2)$ process in heavy-ion collisions.

The study of photon distributions within the nucleus has a long history. Initially, the equivalent photon approximation (EPA), also known as the Weizsäcker-Williams (WW) approximation method [88, 89], is the most commonly used method for addressing photon distribution. In this method, photons are treated as quasi-real particles, and by calculating the lowest-order contributions in QED, one can obtain a photon distribution with low virtuality and transverse momentum. However, the original approximation does not account for both the transverse momentum and the impact parameter of the photon. Recently, inspired by the implementation of the Wigner distribution in QCD studies [93–95], the generalized equivalent photon approximation including the transverse momentum and the impact parameter dependence has been proposed to parameterize the photon distribution from high energy nuclei, which is also known as the photon Wigner distribution [38, 39]. Also, one can define the Generalized Transverse Momentum Dependent (GTMD) distribution by Fourier transforming the impact parameter dependence into the momentum space.

As illustrated in the right figure of Fig. 3, the generalized factorization formula for the process following the GTMD in the correlation limit can be cast into

$$\frac{d\sigma}{dy_1 dy_2 d^2 P_\perp d^2 q_\perp d^2 b_\perp} = \frac{1}{(2\pi)^4} \int d^2 b_{1\perp} d^2 b_{2\perp} \delta^2(\vec{b}_\perp - \vec{b}_{1\perp} + \vec{b}_{2\perp}) \int d^2 k_{1T} d^2 k_{2T} \int d^2 \Delta_{1\perp} d^2 \Delta_{2\perp} e^{-i\vec{b}_{1\perp} \cdot \Delta_{1\perp} - i\vec{b}_{2\perp} \cdot \Delta_{2\perp}} \times \Gamma_{ij}(x_1, \vec{k}_{1T}, \vec{\Delta}_{1\perp}) \Gamma_{kl}(x_2, \vec{k}_{2T}, \vec{\Delta}_{2\perp}) \mathcal{H}^{ijkl}(\vec{P}_\perp) \delta^{(2)}(\vec{q}_\perp - \vec{k}_{1T} - \vec{k}_{2T}), \quad (17)$$

where \mathcal{H}^{ijkl} stands for the hard factor, Γ_{ij} and Γ_{kl} represent the 5-dimensional GTMD distribution with the polarization indices i and k of incoming two photons in the scattering amplitude and the polarization indices j and l of photons in conjugate amplitude. These two-dimensional indices run from 1 to 2. To reconstruct the kinematics of the incoming photons, we write the longitudinal momentum fraction of photon per nucleon as $x_1 = \max[p_{1\perp}, p_{2\perp}](e^{y_1} + e^{y_2})/\sqrt{s}$ and $x_2 = \max[p_{1\perp}, p_{2\perp}](e^{-y_1} + e^{-y_2})/\sqrt{s}$. $b_{1\perp}$ and $b_{2\perp}$ stand for the distance of the photon and its corresponding nucleus. $\vec{k}_{1T} = (\vec{k}_{1\perp} + \vec{k}'_{1\perp})/2$ and $\vec{k}_{2T} = (\vec{k}_{2\perp} + \vec{k}'_{2\perp})/2$ are transverse momenta of two photons, where $k_{i\perp}$ and $k'_{i\perp}$ are the transverse momenta of incoming photons in the amplitude and conjugate amplitude, respectively. According to the momentum conservation, these momenta satisfy $\vec{q}_\perp = \vec{k}_{1\perp} + \vec{k}_{2\perp} = \vec{k}'_{1\perp} + \vec{k}'_{2\perp}$. $\vec{\Delta}_{1\perp} = \vec{k}'_{1\perp} - \vec{k}_{1\perp}$ and $\vec{\Delta}_{2\perp} = \vec{k}'_{2\perp} - \vec{k}_{2\perp}$ are defined as the momentum difference for the nucleus state in the non-forward scatterings and the momentum conservation implies $\vec{\Delta}_{1\perp} + \vec{\Delta}_{2\perp} = 0$. Thus we define $\vec{\Delta}_\perp = \vec{\Delta}_{1\perp} = -\vec{\Delta}_{2\perp}$ for convenience. It is important to note that the momenta from the scattering amplitude and conjugate amplitude only become identical in forward scattering with $\Delta_{1\perp} = \Delta_{2\perp} = 0$. By integrating over the two delta functions, the cross-section can be rewritten as

$$\frac{d\sigma}{dy_1 dy_2 d^2 P_\perp d^2 q_\perp d^2 b_\perp} = \frac{1}{(2\pi)^2} \int d^2 k_{1\perp} d^2 k'_{1\perp} e^{i\vec{b}_\perp \cdot \Delta_\perp} \Gamma_{ij}(x_1, \vec{k}_{1T}, \vec{\Delta}_\perp) \Gamma_{kl}(x_2, \vec{k}_{2T}, -\vec{\Delta}_\perp) \mathcal{H}^{ijkl}(\vec{P}_\perp), \quad (18)$$

with $\vec{\Delta}_\perp = \vec{k}'_{1\perp} - \vec{k}_{1\perp} = \vec{k}_{2\perp} - \vec{k}'_{2\perp}$. By using the definition

$$\Gamma_{ij}(x, \vec{k}_T, \vec{\Delta}_\perp) = \int d^2 b_\perp e^{-i\vec{b}_\perp \cdot \vec{\Delta}_\perp} \Gamma_{ij}(x, \vec{k}_T, \vec{b}_\perp), \quad (19)$$

where b_\perp is the distance of the photon and center of the nucleus, one can convert the GTMD photon distribution into the photon Wigner distribution via the Fourier transform. Then, the generalized factorization formula involving the Winger photon distribution becomes

$$\frac{d\sigma}{dy_1 dy_2 d^2 p_{1\perp} d^2 p_{2\perp} d^2 b_\perp} = \int d^2 b_{1\perp} d^2 b_{2\perp} \delta^2(\vec{b}_\perp - \vec{b}_{1\perp} + \vec{b}_{2\perp}) \int d^2 k_{1T} d^2 k_{2T} \times \Gamma_{ij}(x_1, \vec{k}_{1T}, \vec{b}_{1\perp}) \Gamma_{kl}(x_2, \vec{k}_{2T}, \vec{b}_{2\perp}) \mathcal{H}^{ijkl}(\vec{P}_\perp) \delta^{(2)}(\vec{p}_{1\perp} + \vec{p}_{2\perp} - \vec{k}_{1T} - \vec{k}_{2T}). \quad (20)$$

In the meantime, with the definition

$$\Gamma_{ij}(x, \vec{k}_T, \vec{b}_\perp) = \int d^2 r_\perp e^{-i\vec{k}_T \cdot \vec{r}_\perp} \Gamma_{ij}(x, \vec{r}_\perp, \vec{b}_\perp), \quad (21)$$

where r_\perp represents photon position difference between the amplitude and conjugate amplitude. The cross-section in the full coordinate space can be written as

$$\frac{d\sigma}{dy_1 dy_2 d^2 P_\perp d^2 q_\perp d^2 b_\perp} = \int d^2 b_{1\perp} d^2 r_\perp e^{-iq_\perp \cdot r_\perp} \Gamma_{ij}(x_1, \vec{r}_\perp, \vec{b}_{1\perp}) \Gamma_{kl}(x_2, \vec{r}_\perp, -\vec{b}_\perp + \vec{b}_{1\perp}) \mathcal{H}^{ijkl}(\vec{P}_\perp). \quad (22)$$

In order to derive the hard factor \mathcal{H}^{ijkl} , one needs to carry out the Feynman graph calculation for $\gamma\gamma \rightarrow l^+l^-$ with open indices for all four photon polarizations. After some tedious tensor manipulations, one can eventually find

$$\begin{aligned} \mathcal{H}^{ijkl}(\vec{P}_\perp) = & \frac{\alpha_{\text{em}}^2}{\hat{s}^2} \left\{ 2 \frac{(m_l^4 - \hat{t}\hat{u})(6m_l^4 - 4m_l^2\hat{t} - 4m_l^2\hat{u} + \hat{t}^2 + \hat{u}^2)}{(m_l^2 - \hat{t})^2(m_l^2 - \hat{u})^2} (\delta^{ij}\delta^{kl} - \delta^{ik}\delta^{jl} + \delta^{il}\delta^{jk}) \right. \\ & + \frac{4m_l^4(2m_l^2 - \hat{t} - \hat{u})^2}{(m_l^2 - \hat{t})^2(m_l^2 - \hat{u})^2} (-\delta^{ij}\delta^{kl} + \delta^{ik}\delta^{jl} + \delta^{il}\delta^{jk}) \\ & - \frac{2m_l^2(\hat{t} + \hat{u})(2m_l^2 - \hat{t} - \hat{u})^2}{(m_l^2 - \hat{t})^2(m_l^2 - \hat{u})^2} (\delta^{ij}\delta^{kl} + \delta^{ik}\delta^{jl} - \delta^{il}\delta^{jk}) \\ & - 8m_l^2 \frac{(2m_l^2 - \hat{t} - \hat{u})(m_l^4 - \hat{t}\hat{u})}{(m_l^2 - \hat{t})^2(m_l^2 - \hat{u})^2} \left[\delta^{ij}\Pi^{kl}(\vec{P}_\perp) + \Pi^{ij}(\vec{P}_\perp)\delta^{kl} \right] \\ & \left. - 4 \frac{(m_l^4 - \hat{t}\hat{u})^2}{(m_l^2 - \hat{t})^2(m_l^2 - \hat{u})^2} \Omega^{ijkl}(\vec{P}_\perp) \right\}, \quad (23) \end{aligned}$$

where \hat{s} , \hat{u} and \hat{t} are the Mandelstam variables. Inside the curly brackets, the first three terms are the isotropic contributions which are independent of the orientation of \vec{P}_\perp , the fourth term gives rise to the $\cos(2\phi_P)$ angular correlation, and the last term can generate the $\cos(4\phi_P)$ angular correlation. The tensors $\Pi^{ij}(\vec{P}_\perp)$ and $\Omega^{ijkl}(\vec{P}_\perp)$ are defined as $\Pi^{ij}(\vec{P}_\perp) = 2 \frac{P_\perp^i P_\perp^j}{P_\perp^2} - \delta^{ij}$ and $\Omega^{ijkl}(\vec{P}_\perp) = 2\Pi^{ij}(\vec{P}_\perp)\Pi^{kl}(\vec{P}_\perp) - (\delta^{il}\delta^{jk} + \delta^{ik}\delta^{jl} - \delta^{ij}\delta^{kl})$. They can project the cross-sections onto $\cos(2\phi_P)$ and $\cos(4\phi_P)$ azimuthal angular correlations, respectively. For example, with four arbitrary two-dimensional unit vector $\hat{n}_{1,2,3,4}$, one can obtain

$$\Pi^{ij}\hat{n}_{1i}\hat{n}_{2j} = \cos(\phi_1 + \phi_2 - 2\phi_P), \quad (24)$$

$$\Omega^{ijkl}\hat{n}_{1i}\hat{n}_{2j}\hat{n}_{3k}\hat{n}_{4l} = \cos(\phi_1 + \phi_2 + \phi_3 + \phi_4 - 4\phi_P), \quad (25)$$

where ϕ_1 represents the azimuthal angle orientation of \hat{n}_1 , and similarly for other azimuthal angles.

If we average over the angle of impact parameter b_\perp and project $\cos(2\phi_P)$ terms into $\cos(2\phi_P - 2\phi_q)$ and $\cos(4\phi_P)$ term into $\cos(4\phi_P - 4\phi_q)$, we can reproduce the result derived in Refs. [53]. Since the contribution of lepton mass is power suppressed by factors of m_l^2/P_\perp^2 , we neglect the mass of lepton effect in the hard factor. Then, the hard factor can be significantly simplified and it reads

$$\mathcal{H}^{ijkl}(\vec{P}_\perp) = \frac{\alpha_{\text{em}}^2}{\hat{s}^2} \left[O^{ijkl} - 4\Omega^{ijkl}(\vec{P}_\perp) \right], \quad (26)$$

with

$$O^{ijkl} = 2 \left(\frac{\hat{u}}{\hat{t}} + \frac{\hat{t}}{\hat{u}} \right) (\delta^{ij}\delta^{kl} - \delta^{ik}\delta^{jl} + \delta^{il}\delta^{jk}), \quad (27)$$

$$\Omega^{ijkl}(\vec{P}_\perp) = 2\Pi^{ij}(\vec{P}_\perp)\Pi^{kl}(\vec{P}_\perp) - (\delta^{il}\delta^{jk} + \delta^{ik}\delta^{jl} - \delta^{ij}\delta^{kl}). \quad (28)$$

The terms related to $\cos(2\phi_P)$ are proportional to the lepton's mass, thus they vanish in the massless limit. In the remaining terms, the Ω^{ijkl} term represents the isotropic component with respect to P_\perp and coincides with the angle-averaged ϕ_P term as discussed in Ref. [39]. This term emerges from the contributions of both the unpolarized and the linearly-polarized photon distributions. The $\Omega^{ijkl}(\vec{P}_\perp)$ term, which originates from the interaction between two linearly-polarized photons, will generate the $\cos(4\phi_P)$ angular correlations in the following calculations.

In general, the GTMD photon distribution can be parametrized as follows

$$\Gamma^{ij}(x, \vec{k}_T, \vec{\Delta}_\perp) = \frac{\delta^{ij}}{2} x f_\gamma(x, \vec{k}_T, \vec{\Delta}_\perp) + \left(\frac{k_+^i k_-^j}{\vec{k}_- \cdot \vec{k}_+} - \frac{\delta^{ij}}{2} \right) x h_\gamma(x, \vec{k}_T, \vec{\Delta}_\perp), \quad (29)$$

with $\vec{k}_\pm = \vec{k}_\perp \pm \vec{\Delta}_\perp/2$. The first term represents the unpolarized photon distribution and the second term stands for linearly-polarized photon distribution. We can assume that the unpolarized photon distribution is the same as the linearly-polarized photon distribution, and the GTMD photon distribution can be parametrized as

$$\Gamma^{ij}(x_1, \vec{k}_{1T}, \vec{\Delta}_\perp) = \frac{Z^2 \alpha_{\text{em}}}{\pi^2} k_{1\perp}^i k'_{1\perp}^j \frac{F_A(k_1)}{k_1^2} \frac{F_A(k'_1)}{k'^2_1}, \quad (30)$$

where $F_A(k_1)$ is the normalized elastic charge form factor for the nucleus, Z is charge number of nucleus and m_p is the mass of proton with $k_1^2 = x_1^2 m_p^2 + k_{1\perp}^2$ and $k'^2_1 = x'^2_1 m_p^2 + k'^2_{1\perp}$. Now, the cross-section also can be written as

$$\begin{aligned} \frac{d\sigma}{dy_1 dy_2 d^2 P_\perp d^2 q_\perp d^2 b_\perp} &= \frac{1}{(2\pi)^2} \frac{2\alpha_e^4}{\hat{s}^2} \left(\frac{Z^2}{\pi^2} \right)^2 \int d^2 k_{1\perp} d^2 k'_{1\perp} e^{ib_\perp \cdot \Delta_\perp} \frac{F_A(k_1)}{k_1^2} \frac{F(k_2)}{k_2^2} \frac{F_A(k'_1)}{k'^2_1} \frac{F_A(k'_2)}{k'^2_2} k_{1\perp} k'_{1\perp} k_{2\perp} k'_{2\perp} \\ &\times \left[\left(\frac{\hat{u}}{\hat{t}} + \frac{\hat{t}}{\hat{u}} \right) \cos(\phi_{k_{1\perp}} - \phi_{k'_{1\perp}} + \phi_{k_{2\perp}} - \phi_{k'_{2\perp}}) - 2 \cos(\phi_{k_{1\perp}} + \phi_{k'_{1\perp}} + \phi_{k_{2\perp}} + \phi_{k'_{2\perp}} - 4\phi_P) \right]. \end{aligned} \quad (31)$$

From the above equation, by averaging over the impact parameter angle b_\perp and projecting the $\cos(4\phi_P)$ term into $\cos(4\phi_P - 4\phi_q)$ direction, we can reproduce the results derived in Refs. [38]. In the coordinate space, if we integrate over q_\perp and ϕ_q and implement the delta function track in the anisotropy term, it is straightforward to find that the above equation is equal to the results given by Eq. (5) in Ref. [41]. One can find that all anisotropic terms with ϕ_q disappear, and only $\cos(4\phi_b - 4\phi_P)$ remains.

The cross-section, indicative of the interaction probability between particles, must be positively defined. As mentioned in Ref. [39], the photon GTMD is not always positive definite. Consequently, it is essential to demonstrate that dilepton production via photon-photon fusion is invariably guaranteed to yield a positive definite cross-section. Based on Eq. (31), it is interesting to show that

$$\begin{aligned} \frac{d\sigma}{dy_1 dy_2 d^2 P_\perp d^2 q_\perp d^2 b_\perp} &\geq \frac{1}{(2\pi)^2} \left(\frac{Z^2}{\pi^2} \right)^2 \int d^2 k_{1\perp} d^2 k'_{1\perp} e^{ib_\perp \cdot \Delta_\perp} \frac{F_A(k_1)}{k_1^2} \frac{F(k_2)}{k_2^2} \frac{F_A(k'_1)}{k'^2_1} \frac{F_A(k'_2)}{k'^2_2} k_{1\perp} k'_{1\perp} k_{2\perp} k'_{2\perp} \\ &\times \frac{4\alpha_e^4}{\hat{s}^2} [\cos(\phi_{k_{1\perp}} - \phi_{k'_{1\perp}} + \phi_{k_{2\perp}} - \phi_{k'_{2\perp}}) - \cos(\phi_{k_{1\perp}} + \phi_{k'_{1\perp}} + \phi_{k_{2\perp}} + \phi_{k'_{2\perp}} - 4\phi_P)] \end{aligned} \quad (32)$$

By using the following identities

$$\begin{aligned} &2 \sin(\phi_{k_{1\perp}} + \phi_{k_{2\perp}} - 2\phi_P) \sin(\phi_{k'_{1\perp}} + \phi_{k'_{2\perp}} - 2\phi_P) \\ &= \cos(\phi_{k_{1\perp}} - \phi_{k'_{1\perp}} + \phi_{k_{2\perp}} - \phi_{k'_{2\perp}}) - \cos(\phi_{k_{1\perp}} + \phi_{k'_{1\perp}} + \phi_{k_{2\perp}} + \phi_{k'_{2\perp}} - 4\phi_P), \end{aligned} \quad (33)$$

and

$$\sin(\phi_{k_{1\perp}} + \phi_{k_{2\perp}} - 2\phi_P) = \sin(\phi_{k_{1\perp}} - \phi_P) \cos(\phi_{k_{2\perp}} - \phi_P) + \cos(\phi_{k_{1\perp}} - \phi_P) \sin(\phi_{k_{2\perp}} - \phi_P), \quad (34)$$

one can rewrite the cross section as

$$\frac{d\sigma}{dy_1 dy_2 d^2 P_\perp d^2 q_\perp d^2 b_\perp} \geq \left(\frac{Z^2}{\pi^2} \right)^2 \frac{8\alpha_e^4}{(2\pi)^2 \hat{s}^2} (G^{12} + G^{21}) (G^{12*} + G^{21*}), \quad (35)$$

where we define unit vector \hat{l}_i which has the angle $\phi_{l_i} = \phi_{k_{i\perp}} - \phi_P$ and G^{ik} is defined as $G^{ik} = \int d^2 k_{1\perp} e^{ik_{1\perp} \cdot b_\perp} F_A(k_1) F_A(k_2) |k_{1\perp}| |k_{2\perp}| \hat{l}_1^i \hat{l}_2^k$. It is then obvious to see that the cross-section is positive definite, since the right hand side is essentially related to the square of an amplitude.

2. Phenomenological Studies

Based on the above unified GTMD factorized framework, we discuss phenomenological studies of dilepton production in this subsection in detail. First, we elaborate on the various dilepton anisotropies and show the numerical predictions. Then, we include the Sudakov effect, which resums the soft photon radiation emitted by the lepton pairs. In addition, we take the neutron emission effect in ultra-peripheral collisions (UPCs) into account. Finally, we discuss the incoherent contribution of the photon Wigner distribution.

a. Anisotropies

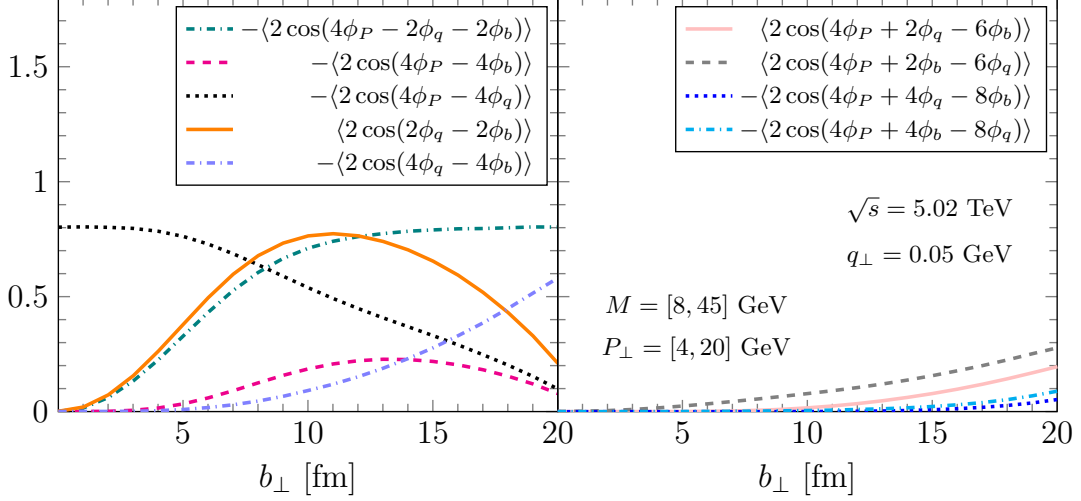


FIG. 4. The prediction of different dilepton anisotropies as a function of b_{\perp} with pair mass $M = 8 - 45$ GeV, fixed $q_{\perp} = 0.05$ GeV and $P_{\perp} = 4 - 20$ GeV at the LHC kinematics. The rapidities of the dilepton are integrated over the regions $[-1, 1]$.

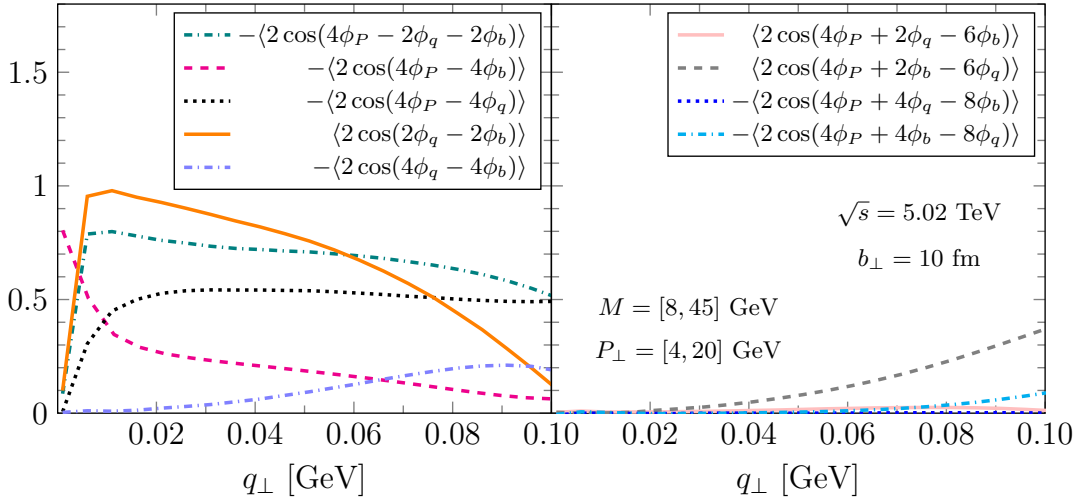


FIG. 5. Predictions of different dilepton anisotropies are presented as a function of q_{\perp} for a pair mass $M = [8, 45]$ GeV, with b_{\perp} fixed at 10 fm and P_{\perp} ranging from 4 to 20 GeV, within the LHC kinematics. The rapidities of the dileptons are integrated over the interval $[1, 1]$.

In the following, we explore the anisotropy of the dilepton production process $\gamma + \gamma \rightarrow l^+ + l^-$. The cross-section contains various anisotropies. For example, there are a lot of studies about the angular correlation between P_{\perp} and

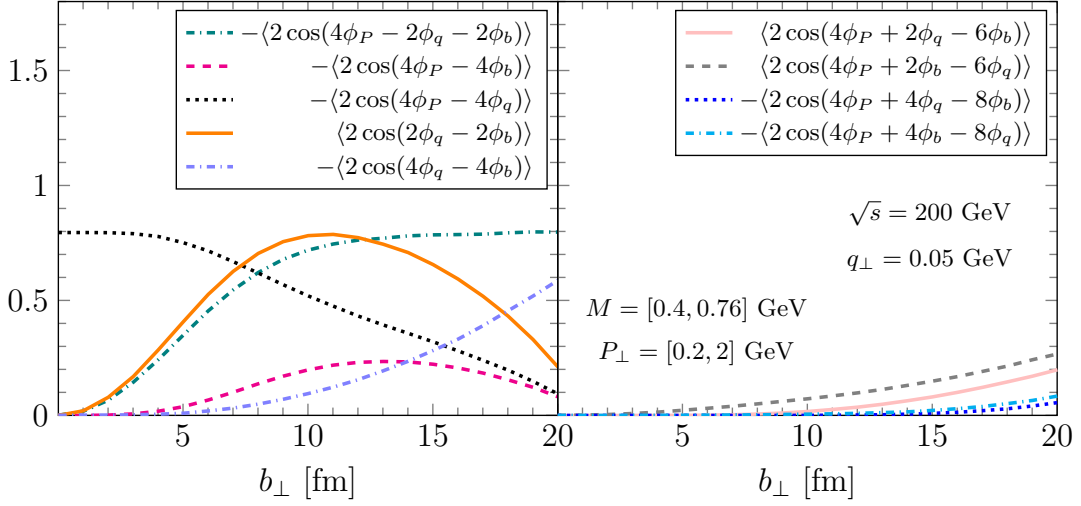


FIG. 6. Under RHIC kinematics, the anisotropies of dileptons are predicted as functions of b_{\perp} , with the pair mass M ranging from 0.4 to 0.76 GeV, q_{\perp} fixed at 0.05 GeV, and P_{\perp} between 0.2 and 2 GeV. The rapidities of the dileptons are integrated over the interval $[-1, 1]$.

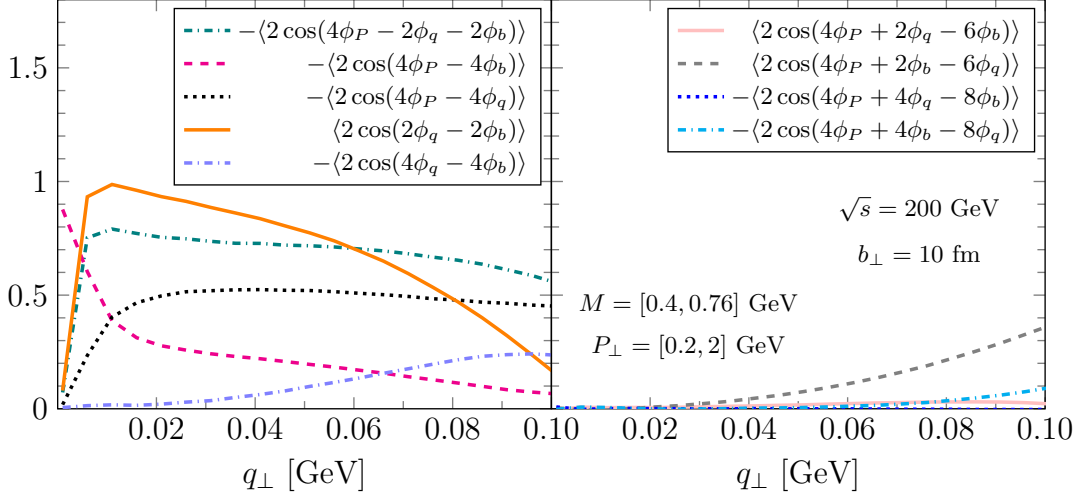


FIG. 7. For RHIC kinematics, the anisotropies of dileptons are predicted as functions of q_{\perp} , with the pair mass M ranging from 0.4 to 0.76 GeV, b_{\perp} fixed at 10 fm, and P_{\perp} between 0.2 and 2 GeV. The rapidities of the dileptons are integrated over the interval $[-1, 1]$.

b_{\perp} , and the angular correlation between P_{\perp} and q_{\perp} , which results in the commonly measured $\cos(4\phi_P - 4\phi_q)$ and α distribution, as shown in Refs. [37–41, 43–45, 53, 55].

Based on the expression of the hard factor $\mathcal{H}^{ijkl}(\vec{P}_{\perp})$ in Eq. (26) and its projection properties when contracting with the impact parameter (\vec{b}_{\perp}) and the transverse momentum of the final lepton pair (\vec{q}_{\perp}), we can project the cross-section in the following general Fourier harmonic series

$$\begin{aligned} \sigma = & \sigma_0 + \sigma_{2qb} \cos(2\phi_q - 2\phi_b) + \sigma_{4qb} \cos(4\phi_q - 4\phi_b) + \sigma_{4qP} \cos(4\phi_q - 4\phi_P) \\ & + \sigma_{4bP} \cos(4\phi_b - 4\phi_P) + \sigma_{qbP} \cos(2\phi_q + 2\phi_b - 4\phi_P) + \dots, \end{aligned} \quad (36)$$

where the harmonic coefficients $\sigma_{2qb}, \sigma_{4qb}, \dots$ contains the detailed quantum information of the photon flux. From the GTMD factorization framework, we find that linearly polarized photons can generate various anisotropies with considerable magnitudes from the correlation among azimuthal angles of q_{\perp} , P_{\perp} , and b_{\perp} . Not only can we reproduce anisotropies studied in the previous works, but we have also found several other interesting correlations arising from the inner products of P_{\perp} , q_{\perp} and b_{\perp} . These anisotropies can be divided into two categories.

The first category of correlation is independent of P_\perp . When the O^{ijkl} term from the hard factor $\mathcal{H}^{ijkl}(\vec{P}_\perp)$, an isotropic term associated with P_\perp , couples with two incoming Wigner photon distributions, it results in two significant angular correlations: $\cos(2\phi_q - 2\phi_b)$ and $\cos(4\phi_q - 4\phi_b)$. More precisely, when we analyze the cross-section in momentum space, these correlations originate from the contraction between the hard factor and the linearly polarized photon distribution via the phase factor $e^{i\vec{b}_\perp \cdot \vec{\Delta}_\perp}$. This second category involves the $\cos(4\phi_P)$ harmonics, which comes from the tensor contraction between the $\Omega^{ijkl}(\vec{P}_\perp)$ term in the hard factor and the incoming linearly polarized photon distributions. Two anisotropies proposed in Refs [37, 41], namely $\cos(4\phi_P - 4\phi_q)$ and $\cos(4\phi_P - 4\phi_b)$, originate from this mechanism and belong to this category. In addition, we also find that the same mechanism can give rise to several novel angular correlation of three final observables P_\perp , q_\perp , and b_\perp , such as $\cos(4\phi_P - 2\phi_q - 2\phi_b)$, $\cos(4\phi_P - 6\phi_q + 2\phi_b)$, and $\cos(4\phi_P - 6\phi_b + 2\phi_q)$, and etc.

To extract the harmonic coefficients, we can use the following definition and compute the average value of the harmonics $\cos(\dots)$

$$2\langle \cos(\dots) \rangle = \frac{2 \int d\mathcal{P} \cdot \mathcal{S} \cdot \cos(\dots) \frac{d\sigma}{dy_1 dy_2 d^2 P_\perp d^2 q_\perp d^2 b_\perp}}{\int d\mathcal{P} \cdot \mathcal{S} \cdot \frac{d\sigma}{dy_1 dy_2 d^2 P_\perp d^2 q_\perp d^2 b_\perp}}, \quad (37)$$

where $\int d\mathcal{P} \cdot \mathcal{S}$ represents the phase space integrals. In computing the angular correlations with given q_\perp and b_\perp , we define it as $\int dy_1 dy_2 d^2 P_\perp d\phi_q d\phi_b$. We show predictions for the anisotropies as a function of b_\perp with fixed $q_\perp = 50$ MeV at the LHC in the Fig. 4. As shown in these plots, we find that there are nine azimuthal angular correlations, which are numerically significant. As discussed above, the first category includes two angular correlation terms $2\langle \cos(2\phi_q - 2\phi_b) \rangle$ and $2\langle \cos(4\phi_q - 4\phi_b) \rangle$. $2\langle \cos(2\phi_q - 2\phi_b) \rangle$ has a sizeable positive contribution. As the impact parameter b_\perp increases, it increases in the region $b_\perp < 2R_A$, and peaks at $2R_A$, then decreases in the region $b > 2R_A$. The $2\langle \cos(4\phi_q - 4\phi_b) \rangle$ term is usually negative, and its magnitude increases as the impact parameter b_\perp increases.

The second category of the correlations are related to the $\cos(4\phi_P)$ harmonics, and it can be further subdivided into three different types. The first type is the angular correlations between P_\perp and q_\perp . It includes one angular correlation term, i.e., $2\langle \cos(4\phi_P - 4\phi_q) \rangle$. The second type is the angular correlation between P_\perp and b_\perp , namely, $2\langle \cos(4\phi_P - 4\phi_b) \rangle$. There are lots of related discussions found in Refs. [37, 38, 41, 53, 55] about these two types of correlations. The last type is the angular correlation that mixes all three vectors, q_\perp , b_\perp , and P_\perp . Here, we show five angular correlations as examples. Among them, the $2\langle \cos(4\phi_P - 2\phi_q - 2\phi_b) \rangle$ term has the largest magnitude. This correlation is negative and its magnitude increases as the impact parameter b_\perp increases, and the value tends to be constant in the region $b > 2R_A$. $2\langle \cos(4\phi_P + 2\phi_b - 6\phi_q) \rangle$ and $2\langle \cos(4\phi_P + 2\phi_q - 6\phi_b) \rangle$ are positive, while $2\langle \cos(4\phi_P + 4\phi_b - 8\phi_q) \rangle$ and $2\langle \cos(4\phi_P + 4\phi_q - 8\phi_b) \rangle$ are negative. The amplitudes of these four terms all show similar behaviour, and they increase as the impact parameter b_\perp increases. Similarly, as shown in the Fig. 5, we can find that these anisotropies show similar magnitude as the function of q_\perp at fixed $b = 10$ fm in the LHC.

At a distance of $b = 10$ fm, the colliding nuclei undergo peripheral collisions, which also generates a large number of hadrons. Consequently, the reaction plane of the hadronic events can be used to determine the impact parameter vector \vec{b}_\perp in peripheral collisions. By combining the hadronic reaction plane information with the dilepton measurements, it becomes possible to measure various dilepton angular correlations between b_\perp and q_\perp , P_\perp in peripheral collisions.

In addition, we show predictions about anisotropies as a function of b_\perp and q_\perp at RHIC energy in Fig. 6 and Fig. 7. In these predictions, we determine the values of the pair mass M , the relative transverse momentum of the lepton pair P_\perp , and the rapidity region based on the relevant kinematic region on RHIC and LHC. Although the kinematics are different at the RHIC and LHC, the longitudinal momentum fractions at different energies are almost identical, and the photon Wigner distributions at different energies are comparable. Therefore, we can see that the predictions show very similar behaviors at the RHIC and LHC. In principle, there are infinite number of correlations in this series. We only plot the nine examples of the angular correlations in the above plots. In the future, it would be interesting to compare our results with RHIC and the LHC measurements and it will help us to understand the property of the photon Wigner distribution. We note that the mass effect has been neglected. If one consider the mass effect, more correlation can be observed. We leave it for future study.

b. The Sudakov Effect

This subsection will discuss the effect of multiple soft-photon radiation, which is also known as the Sudakov soft radiation effect. These soft radiations give rise to large logarithms that must be resummed. The resummation improved cross-section is given as [32, 39, 46, 53, 55]

$$\frac{d\sigma}{\pi db_\perp^2 d^2 q_\perp d^2 P_\perp} = \int d^2 l_\perp \mathcal{S}(l_\perp, Q, m_l) \frac{d\sigma}{\pi db_\perp^2 d^2 q'_\perp d^2 P_\perp} (q'_\perp = q_\perp - l_\perp). \quad (38)$$

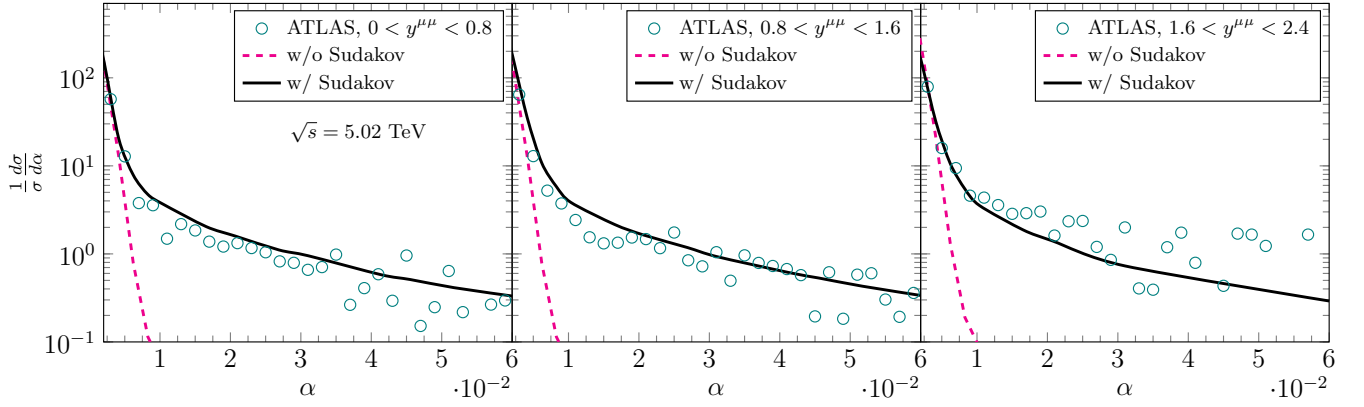


FIG. 8. Comparisons our results with the ATLAS experimental data [4] in the dimuon pair acoplanarity α distribution in UPCs.

As shown in Refs. [39, 55], the Sudakov factor at the leading double logarithm order in the center-of-mass frame of the final lepton pair reads

$$\mathcal{S}(r_{\perp}, Q, m_l) = \frac{\alpha_{\text{em}}}{2\pi} \left[\ln^2 \frac{Q^2 r^2}{c_0^2} - \ln^2 \frac{m_l^2 r^2}{c_0^2} \theta(m_l^2 - r^2/c_0^2) \right]. \quad (39)$$

with the lepton mass m_l and $\alpha_{\text{em}} = 1/137$. As shown in Ref. [39], the resummation has an analytic form in the momentum space, which can be expressed as follows

$$\mathcal{S}(l_{\perp}, Q, m_l) = \int \frac{d^2 r_{\perp}}{(2\pi)^2} e^{i l_{\perp} \cdot r_{\perp}} e^{-\frac{Q_0^2 r_{\perp}^2}{4}} e^{-\mathcal{S}_{\alpha}(r_{\perp}, Q, m_l)} \quad (40)$$

$$= \frac{e^{\gamma_0}}{\pi Q_0^2} \left(\frac{c_0^2 Q_0^2}{4Q^2} \right)^{\beta_1} \Gamma(1 - \beta_1) {}_1F_1(1 - \beta_1, 1, -\frac{l_{\perp}^2}{Q_0^2}), \quad (41)$$

with $\beta_1 = \frac{\alpha_{\text{em}}}{\pi} \ln \frac{Q^2}{l_{\perp}^2 + m_l^2}$, $\gamma_0 = \frac{\alpha_{\text{em}}}{2\pi} \ln^2 \frac{Q^2}{m_l^2}$, $c_0 = 2e^{-\gamma_E}$, the Euler constant γ_E , and Hypergeometric function ${}_1F_1$. To suppress the large r_{\perp} contribution and expedite the numerical calculations, we use a Gaussian factor with a Gaussian width $Q_0 = 10$ MeV. As a consistent check, we find that our numerical results is insensitive to the choice of the width as long as Q_0 is kept small.

In Fig. 8, we present our calculations with and without the Sudakov effect compared to the ATLAS data [4]. The Leading Order (LO) calculation could provide a good description of the lepton pair acoplanarity in the small α region and small- q_{\perp} broadening. However, the cross-sections without the Sudakov factor fall too rapidly at large acoplanarity regions. When considering leptons with larger acoplanarity or larger q_{\perp} , one must include the multiple emissions of soft photons. The calculations that include the Sudakov effect better fit the experimental data at large acoplanarity regions. It demonstrates that Sudakov resummation is critical for accurately computing large acoplanarity regions in dilepton production.

c. Dilepton Events with Neutrons Emission

In this section, we focus on the measurements of dilepton production with neutron emissions and explore the resulting bias in the impact parameter and its corresponding connection with the incoherent photon contribution. Recently, there have been many measurements on dilepton production with neutron tagging from the STAR, CMS, and ATLAS Collaborations in UPCs [3, 6, 7, 10]. When an event involves neutron emission, these neutrons, which are almost collinear with the beam direction, can be detected by the Zero Degree Calorimeter (ZDC).

Generally, the number of emitted neutrons depends on the impact parameter b_{\perp} between two heavy ions. As assumed in Ref. [24], the probability of having N neutron emissions follows the Poisson distribution

$$P(N, b_{\perp}) = \frac{1}{N!} [P_s(b_{\perp})]^N \exp[-P_s(b_{\perp})], \quad (42)$$

where $P_s(b_\perp) = S/b_\perp^2$ is the lowest-order probability for an excited nucleus to emit one neutron, and $P(N, b_\perp)$ represents the probability of emitting N neutrons. Here, one uses the parameter S to indicate the strength of neutron emissions. As shown in Ref. [69], the Giant-Dipole Resonance model gives an expression for S as follows

$$S = 5.45 \times 10^{-5} \frac{Z^3(A-Z)}{A^{2/3}} \text{ fm}^2, \quad (43)$$

with $A =$ atomic mass number and Z being the proton number. For Pb-Pb collisions, the above formula gives $S = 108 \text{ fm}^2$. In addition, one may also choose another parametrization $S = 303 \text{ fm}^2$ which includes all additional radiation mechanism for Pb-Pb collisions [70]. These two different prescriptions show different dependency relations between the probability of neutron emission and the impact parameter. They will be referred to as PAR I and PAR II in the subsequent numerical studies, respectively. We find that some observables are sensitive to the integration range of the impact parameter, and we will discuss in detail the effects of these two prescriptions in the next section. Based on the Poisson distribution, we can write the probability of different numbers of neutron emission as follows

$$P_0(b) = \exp[-P_s(b)], \quad (44)$$

$$P_1(b) = P_s(b) \exp[-P_s(b)], \quad (45)$$

$$P_M(b) = 1 - \exp[-P_s(b)], \quad (46)$$

$$P_X(b) = 1 - \exp[-P_s(b)] - P_s(b) \exp[-P_s(b)], \quad (47)$$

where $P_0(b)$ is the probability of no neutron emission, $P_1(b)$ is the probability of one neutron emission, $P_M(b)$ is the probability of at least one neutron emission, and $P_X(b)$ is the probability of at least two neutron emissions.

Furthermore, we can categorize the UPC event into different scenarios according to the number of collinearly emitted neutrons detected in the ZDC on both ends. For example, the scenario $1nXn$ means that exactly one neutron is detected on one ZDC, and at least two neutrons are detected in the other ZDC. $P_{nm}(b)$ is then defined as the combined probability of various type of neutron emissions from both nuclei as a function of impact parameter. We summarize various scenarios in the following table and plot the probability distributions in the right part of Fig. 9. As shown in the plot of the combined probabilities, the neutron emission multiplicity biases toward a small value of the impact parameter. This means that the distance between two colliding nuclei is, on average, smaller in the events with higher neutron multiplicity. Therefore, neutron emissions can be used as a tool to select events with different impact parameters.

	Neutrons emission	$P_{nn}(b)$
1	$0n0n$	$P_{00}(b) = [P_0(b)]^2$
2	$0n1n$	$P_{01}(b) = 2P_0(b)P_1(b)$
3	$0nMn$	$P_{0M}(b) = 2P_0(b)P_M(b)$
4	$0nXn$	$P_{0X}(b) = 2P_0(b)P_X(b)$
5	$1n1n$	$P_{11}(b) = [P_1(b)]^2$
6	$1nXn$	$P_{1X}(b) = 2P_1(b)P_X(b)$
7	$MnMn$	$P_{MM}(b) = [P_M(b)]^2$
8	$XnXn$	$P_{XX}(b) = [P_X(b)]^2$

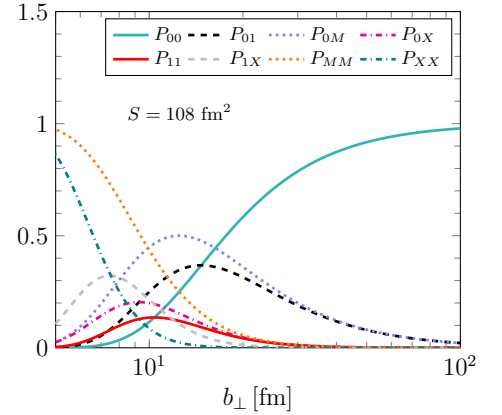


FIG. 9. Left: Table of the combined probability for various neutron emissions. Right: The plot of the combined probabilities as functions of b_\perp .

In addition, to include the effect of neutron emission in our framework, we cast the cross-section into

$$\frac{d\sigma_{nn}}{d^2P_\perp d^2q_\perp} = \int_{b_{\min}}^{\infty} db_\perp b_\perp \int d\phi_b \frac{d\sigma}{d^2b_\perp d^2P_\perp d^2q_\perp} P_{nn}(b_\perp), \quad (48)$$

where b_{\min} is defined as the minimum impact parameter value to distinguish between peripheral collisions and the UPCs. For the case of $0n0n$, we note that the neutron emission probability P_{00} is non-vanishing at large b_\perp , resulting in slow numerical convergence when combined with the phase factor. Since the probability of $P_{00}(b_\perp)$ approaches one

when the impact parameter is much larger than R_A , we can use the following technique to calculate the $0n0n$ case numerically. We first separate the cross-section into two terms as follows

$$\begin{aligned} \frac{d\sigma_{00}}{d^2P_\perp d^2q_\perp} &= \int_{b_{\min}}^{\infty} db_\perp b_\perp \int d\phi_b \frac{d\sigma}{d^2b_\perp d^2P_\perp d^2q_\perp} P_{00}(b_\perp) \\ &= \int_{b_{\min}}^{\infty} db_\perp b_\perp \int d\phi_b \frac{d\sigma}{d^2b_\perp d^2P_\perp d^2q_\perp} - \int_{b_{\min}}^{\infty} db_\perp b_\perp \int d\phi_b \frac{d\sigma}{d^2b_\perp d^2P_\perp d^2q_\perp} [1 - P_{00}(b_\perp)], \end{aligned} \quad (49)$$

where the second term is convergent rapidly in numerical computation, and the first term is the full UPC contribution

$$\frac{d\sigma^{\text{UPC}}}{d^2P_\perp d^2q_\perp} = \int_{b_{\min}}^{\infty} db_\perp b_\perp \int d\phi_b \frac{d\sigma}{d^2b_\perp d^2P_\perp d^2q_\perp}. \quad (50)$$

We can analytically perform the integration over impact parameter from b_{\min} to infinity for σ^{UPC} by following the same technique as suggested in Ref. [39].

d. The Incoherent Contribution to the Photon Distribution

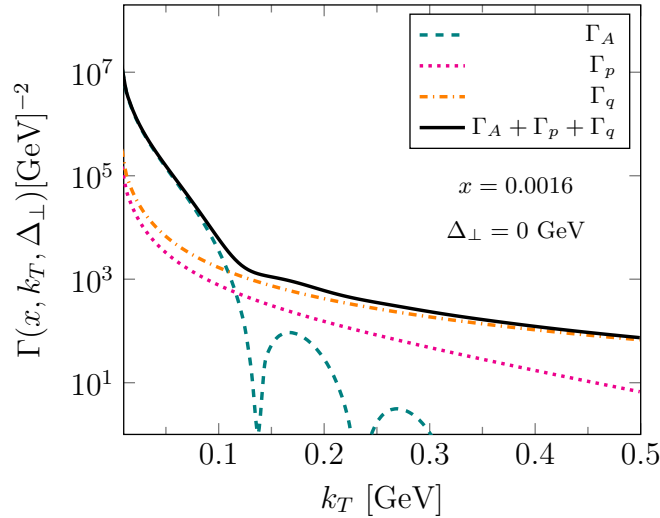


FIG. 10. The illustration of the coherent and incoherent contributions to the GTMD photon distribution, with the coherent nucleus represented by dashed lines, the incoherent proton contribution by dotted lines, and the incoherent quark contribution by dash-dotted lines. The solid lines depict the combined distribution of coherent and incoherent contributions. We set the momentum fraction at $x = 0.0016$ and Δ_\perp to 0 GeV.

Let us discuss the incoherent contributions to the photon distribution and its connection to the neutron emission events. For dilepton production from the photon-photon fusion process, when the momentum imbalance q_\perp of the lepton pair is small compared to $1/R_A$ (where R_A is the radius of the nucleus), the nucleus, as a whole, can be treated as the source of photons. This contribution is commonly referred to as the coherent contribution. However, as the momentum imbalance of the lepton pair increases, the transverse momenta carried by the incoming photons should also increase accordingly. Therefore, according to the uncertainty principle, the photon with large transverse momentum no longer originates solely from the coherent nuclear radiation process but can be emitted from the inner structure of the nucleus, such as the protons or the quarks inside the protons and neutrons. These contributions are known as the incoherent contributions.

If quasi-photons with relatively large transverse momenta are radiated from the interior of heavy nuclei, these emissions can likely lead to the disintegration of these nuclei. Consequently, the structural integrity of the heavy nuclei can serve as a key indicator in determining whether this incoherent interaction occurs or not. As discussed in the above section, lots of experimental data with the neutron emission effect have been observed by STAR, CMS, and ATLAS Collaborations [3, 6, 7, 10]. For the $0n0n$ event, the outgoing nuclei are assumed to still remain intact, thus the dominant contribution is from the coherent photon emissions. In the $MnMn$ and $0nMn$ events in which ZDC can

detect a number of neutrons, the outgoing nuclei are disintegrated, and incoherent photon interactions should take place. Therefore, we should include the incoherent contribution in our framework to provide a complete description of the experimental data with neutron emissions.

To account for the incoherent contributions, it is still reasonable to treat the incoming photon as a quasi-real particle and employ the generalized equivalent photon approximation for the calculation. The only difference is that we are treating the nucleus as an incoherent collection of electric charges. Consequently, considering the coherent and incoherent contributions together, one can modify the corresponding $\Gamma^{ij}(x, k_T, \Delta_\perp)$, and write it as

$$\Gamma^{ij}(x, \vec{k}_T, \vec{\Delta}_\perp) = \Gamma_A^{ij}(x, \vec{k}_T, \vec{\Delta}_\perp) + \Gamma_p^{ij}(x, \vec{k}_T, \vec{\Delta}_\perp) + \Gamma_q^{ij}(x, \vec{k}_T, \vec{\Delta}_\perp), \quad (51)$$

where the first term is the coherent contribution from the nucleus. The second and last terms are the incoherent contributions from the protons and quarks inside nucleons, respectively. When the protons inside the heavy nucleus are viewed as the photon sources, the corresponding total GTMD of the nucleus is given as the incoherent sum of the photon distributions from individual protons

$$\Gamma_p^{ij}(x, \vec{k}_T, \vec{\Delta}_\perp) = Z \frac{\alpha_{em}}{\pi^2} k_\perp^i k_\perp^j \frac{F_p(k)}{k^2} \frac{F_p(k')}{k'^2}, \quad (52)$$

where $F_p(k)$ is the proton form factor. When the photon is radiated incoherently by the quark inside protons or neutrons, we can write the photon GTMD by treating the quarks as point particles, which is presented as follows

$$\Gamma_q^{ij}(x, \vec{k}_T, \vec{\Delta}_\perp) = \left[Z \sum e_{q/p}^2 + (A - Z) \sum e_{q/n}^2 \right] \frac{\alpha_{em}}{\pi^2} k_\perp^i k_\perp^j \frac{1}{k^2} \frac{1}{k'^2}, \quad (53)$$

where e_q is the charge number of quark from protons and neutrons. In the above equation, the first and second terms correspond to the contribution of the quark inside protons and neutrons, respectively. According to the experimental cuts used in the measurement, the transverse momentum imbalance of the final lepton pairs q_\perp is expected to be less than 1.2 GeV, which means the quantum fluctuations within nucleons are comparatively small and the QCD evolution effect may be neglected. Therefore, we can use the valence quark model to simplify the calculation. In this model, a proton comprises two up quarks and one down quark, while a neutron consists of one up quark and two down quarks, with these quarks inside nucleons taking the same momenta.

In our numerical calculations, we employ the following parametrizations of the nuclear form factor [98] $F_A(k) = \frac{3}{(kR_A)^3} \frac{1}{1+a^2k^2} [\sin(kR_A) - kR_A \cos(kR_A)]$, where $a = 0.71$ fm, and $R = 6.6$ fm for Pb and $R = 6.4$ fm for Au and the proton form factor [99, 100] $F_p(k) = \frac{1}{[(k^2/0.71 \text{ GeV}^2)+1]^2}$.

For comparison, we plot three different contributions (coherent, incoherent proton part, and incoherent quark part) to the GTMD photon distribution in Fig. 10. The momentum fraction x in this plot is estimated with $p_{1\perp} = p_{2\perp} = 4$ GeV and $\Delta_\perp = 0$ GeV at midrapidity $y_1 = y_2 = 0$ at LHC energy. We observe that the photon distribution originating from the coherent nucleus Γ_A dominates at low k_T values, while the incoherent contributions are a couple of magnitudes smaller than the coherent nucleus contribution. In the large k_T regime, the coherent contribution Γ_A falls off rather rapidly as k_T increases, and the incoherent distribution becomes much larger than the coherent contribution when $k_T > 0.15$ GeV. Furthermore, the quark contribution to the photon distribution Γ_q is larger than that from protons Γ_p . For the sum of coherent and incoherent contributions, in the small k_\perp regions, the nucleus acts as the dominant photon source, which means the modified GTMD is consistent with the traditional GTMD in the small k_\perp region. In the large k_\perp region, the incoherent distribution from quarks takes over. It is interesting to note that the combined photon GTMD distribution is proportional to Z^2 in the small transverse momentum region and proportional to $(A - Z) \sum e_{q/n}^2 + Z \sum e_{q/p}^2 = \frac{2}{3}(A - Z) + Z$ in the asymptotically large transverse momentum region. The incoherent emission of photons is rare compared to the coherent emission, yet it is more efficient in generating high k_T photons than the coherent emission.

For dilepton production, if the transverse momentum imbalance of the final lepton pairs q_\perp is small, the two colliding initial photons typically possess low transverse momenta, which in turn suggests that the photons originate predominantly from the coherent nucleus. Under such conditions, the photons “see” the nucleus as a whole. Conversely, when q_\perp is large, either or both of the initial photons are likely to have high transverse momenta and are typically emitted by protons or quarks. This means that these high-momentum photons can allow us to perceive the internal structures within the nucleus. Therefore, this incoherent process is likely to excite the nucleus, causing it to emit one or more neutrons in the beam direction, which can subsequently be recorded by the ZDC detector. The incoherent contribution is expected to be the dominant production mechanism for q_\perp broadening in dilepton production for events with one or more neutron emissions, such as $0nMn$ and $MnMn$. In the next section, we will compare our numerical calculations with experimental data involving neutron tagging and show that the inclusion of the incoherent contribution is required if one wishes to describe both the data with and without neutron emissions.

3. Comparisons with the RHIC and LHC data

In this section, we compare our numerical results with the dilepton experimental data collected in a wide variety of measurements. Firstly, we provide a numerical comparison with the acoplanarity and q_{\perp} broadening results. Furthermore, we compare our results with the neutron-tagging data from STAR, CMS, and ATLAS Collaborations. Also, we turn on the incoherent contributions to account for enhancements in the large α region when neutron emissions are detected. To minimize various uncertainty, we choose to normalize both the computed cross-section and the experimental data to unity. In addition, as the measurements conducted thus far have focused solely on the angular correlation at a fixed impact parameter b_{\perp} without specifying its orientation, we integrate over the azimuthal angle of b_{\perp} in the subsequent numerical calculations when comparing with the data.

a. Acoplanarity and Transverse Momentum Broadening

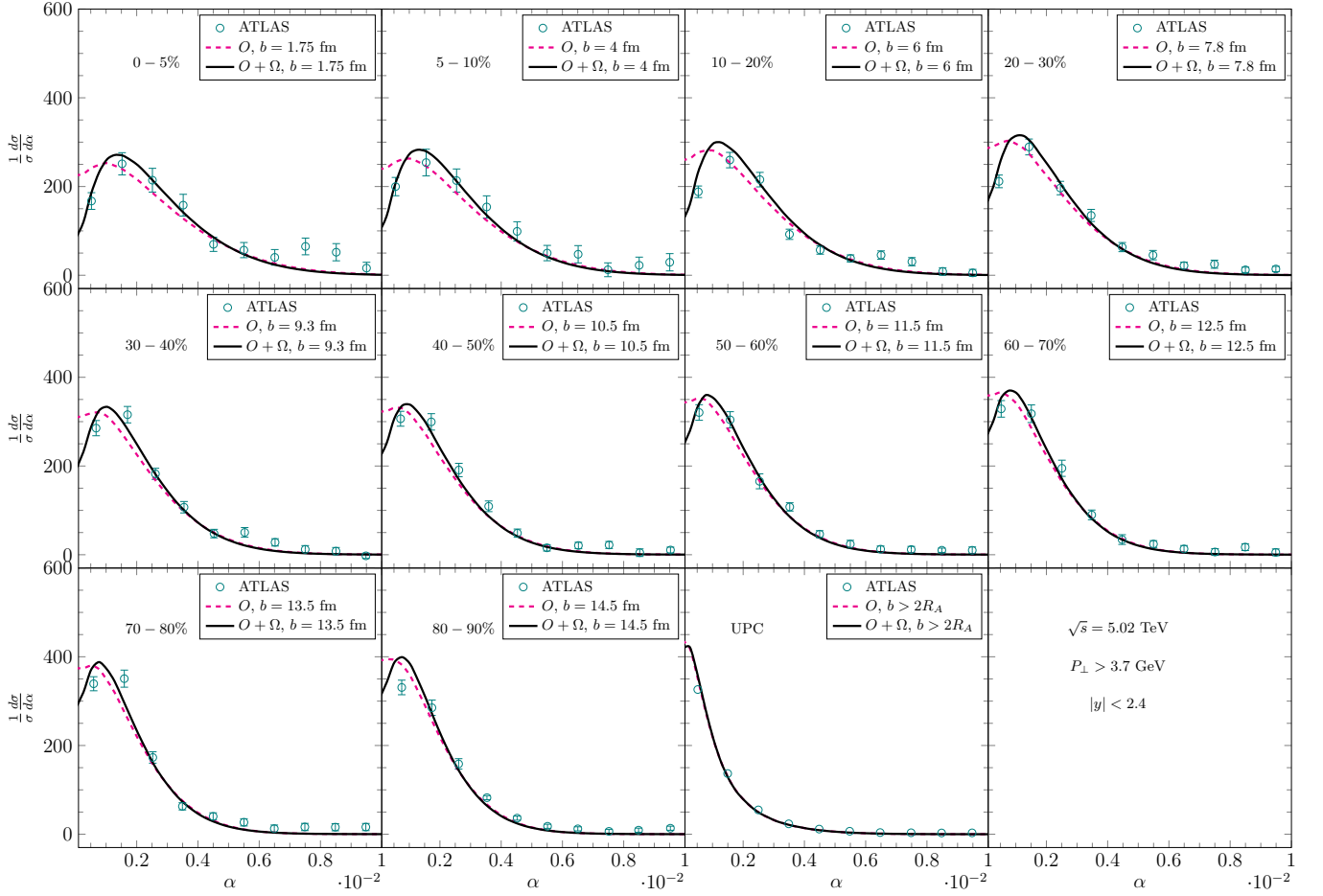


FIG. 11. Comparisons of our results with the ATLAS experimental data [9] in the dimuon pair acoplanarity α distribution from central collisions to UPC.

In this subsection, we provide quantitative analyses on the α distribution and its related observable k_{\perp} in comparison with the ATLAS experimental data. We then further calculate the q_{\perp} distribution and compare it with the STAR measurements for studying the dilepton broadening effects.

The acoplanarity α is the physical observable describing the azimuthal angular correlation between the lepton pairs. It is defined as

$$\alpha = 1 - |\Delta\phi|/\pi, \quad (54)$$

where $\Delta\phi = \phi_1 - \phi_2$ is the angle difference between the azimuthal angle of lepton and anti-lepton ϕ_1 and ϕ_2 . In Fig. 11, we compare our results with the ATLAS experimental data [9] in the dimuon pair acoplanarity α from central

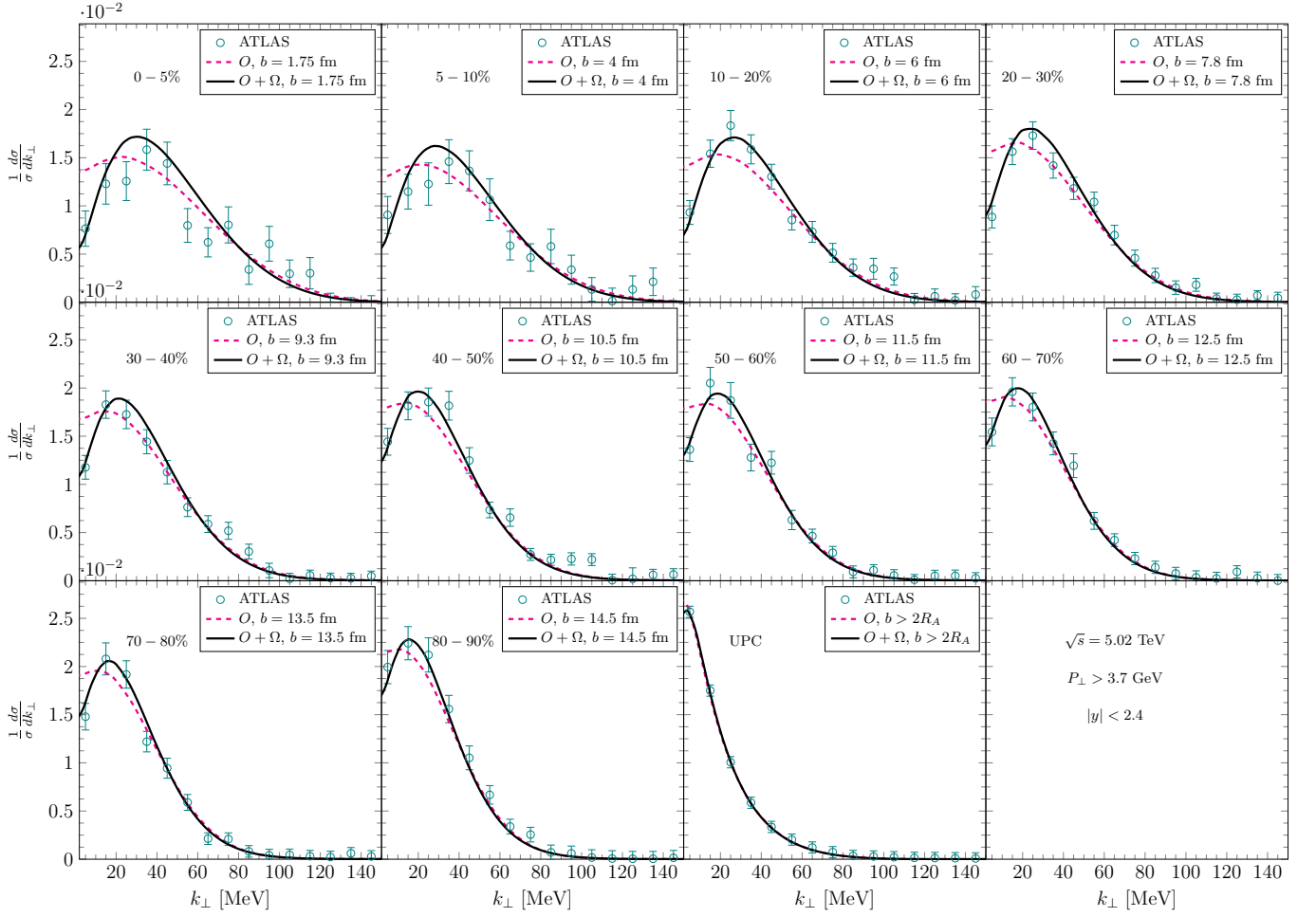


FIG. 12. Comparisons of our results with the ATLAS experimental data [9] in the dimuon pair k_{\perp} distribution from central collisions to UPC.

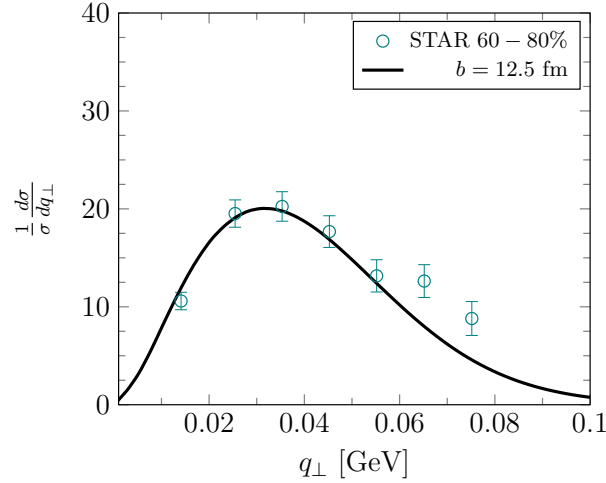


FIG. 13. Comparisons of our results with the STAR experimental data [3] in the dilepton pair transverse momentum imbalance q_{\perp} distribution at 60 – 80% central collisions.

collisions to UPC. The values of the impact parameter corresponding to the different centralities are extracted using the Glauber model. Since the normalized central collision results are almost identical for the impact parameters

$b_{\perp} = 0, 1.75, 3.5$ fm, thus we simply use the average $b_{\perp} = 1.75$ fm for the $0 - 5\%$ centrality bin. One observes that our results can perfectly describe the experimental data. Although the dominant contribution is attributed to the angle average of ϕ_P term O^{ijkl} , it does not capture the dip observed in very small α regions at central collisions. By including the angular correlation $\cos 4\phi_P$ term Ω^{ijkl} , we can describe the dip across various centrality ranges. Hence, the role of the Ω^{ijkl} term is crucial in accurately describing the dip in central collisions. As the impact parameter b_{\perp} increases, the significance of the Ω^{ijkl} term diminishes. Notably, in the case of UPC with large impact parameters, the dominant contribution stems from the O^{ijkl} term, rendering the Ω^{ijkl} term negligible. In addition, we can find that the peak of α distribution is shifted to smaller values of α from central collisions to UPC. We note that these numerical findings can also be derived from the computations in Refs. [35, 37, 38, 48, 50, 55], with this dip arising from the presence of the $\cos 4\Delta\phi$ term.

Besides the α distribution, ATLAS experiments have also used another physical observable k_{\perp} which is closely related to α . This observable can provide us a good estimate of the momentum imbalance and it is defined as

$$k_{\perp} = \pi\alpha P_{\perp}, \quad (55)$$

where P_{\perp} is the relative transverse momentum of the lepton pair. As shown in Fig. 12, we compare our results with the ATLAS experimental data [9] in the dimuon pair acoplanarity k_{\perp} , ranging from central collisions to UPC. Our results offer a good description of the data across a wide range. We observe that the k_{\perp} distribution shows similar behaviours with the α distribution, where the dip at small k_{\perp} for small b_{\perp} can be explained by including the contribution of the anisotropic Ω^{ijkl} term.

Additionally, we present our calculation alongside the STAR experimental data [3], in the transverse momentum imbalance q_{\perp} distribution of dilepton pairs at $60 - 80\%$ central collisions. Our results provide a satisfactory description of the data. Given that the momentum imbalance q_{\perp} is an angle-independent observation, only the average term O^{ijkl} of the hard factor contributes, and the Ω^{ijkl} term of the hard factor vanishes.

Therefore, the above figures show that the dilepton acoplanarity and the broadening of the momentum imbalance q_{\perp} encode the initial photons' transverse momentum information and they allow us to further explore the 5-dimensional photon Wigner distribution function and GTMD.

b. The Neutron Emission effect in the Small α Region

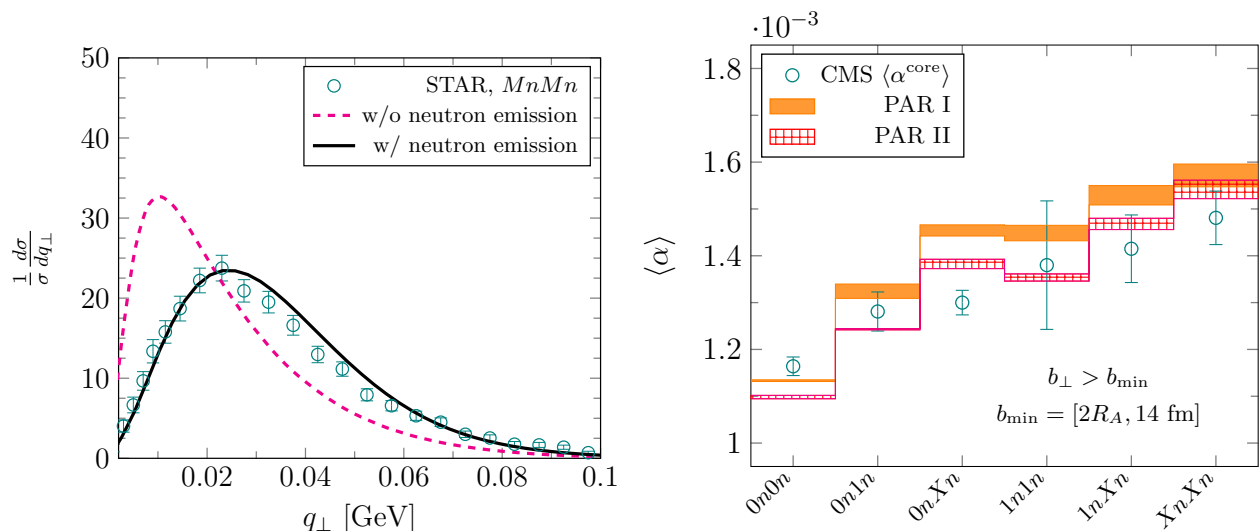


FIG. 14. Left: Comparison of our numerical results for the transverse momentum imbalance q_{\perp} distribution of dilepton pairs, with and without triggering the neutron emission, with the STAR experimental data [3] measured in UPCs with neutron emissions; Right: Comparisons of our results for the dimuon pair $\langle\alpha\rangle$ with the CMS experimental data [7].

In the small α region or low transverse momentum imbalance regime, the neutron multiplicity in UPCs can serve as an indicator of the impact parameter, as more neutron emission biases toward smaller impact parameter. Firstly, we show the impact of neutron emission on the q_{\perp} distribution at RHIC energy. Secondly, we study the average acoplanarity $\langle\alpha\rangle$ distribution measured at CMS Collaboration. The comparisons of our numerical calculations with

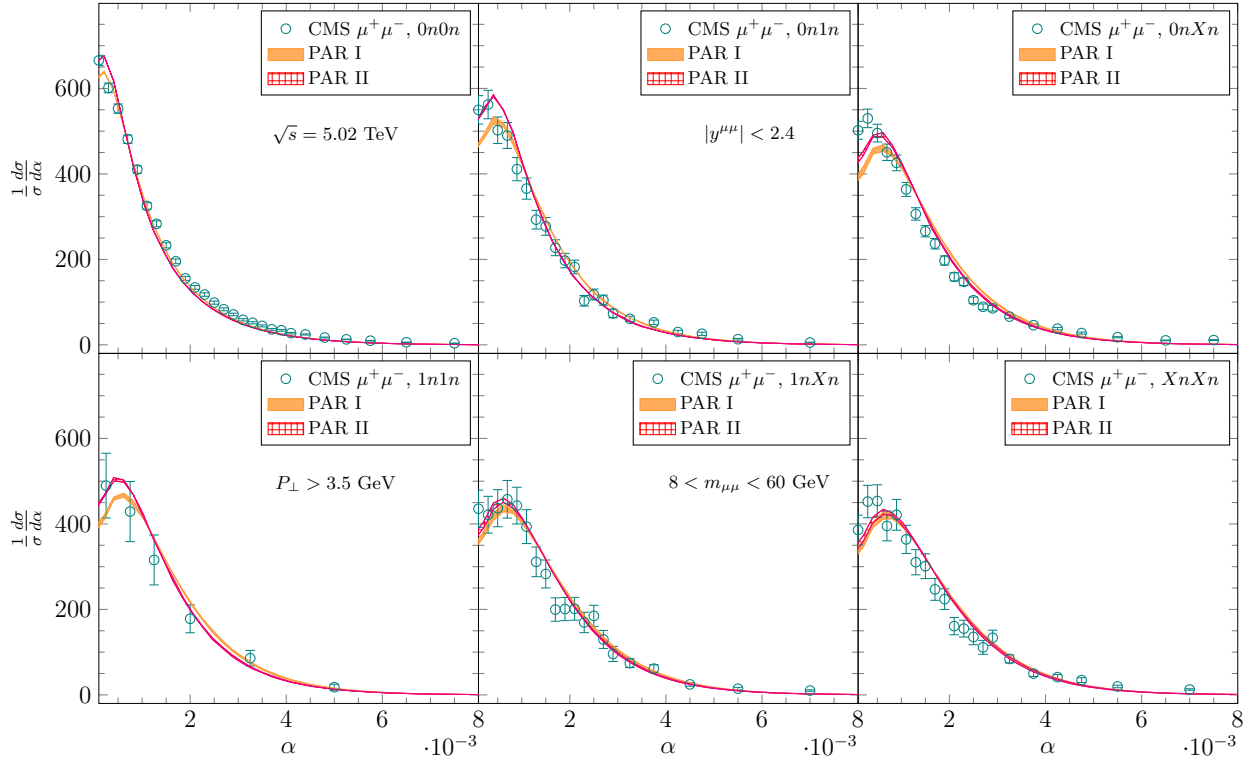


FIG. 15. Comparisons of our results with the CMS experimental data [7] for the dimuon pair acoplanarity α distribution with the neutron emission in UPCs.

the acoplanarity α distribution from CMS Collaboration are also presented for different configurations of neutron emission tags. Lastly, we compare our numerical results with the α distribution measured at ATLAS Collaboration in the large α region.

In the left plot of Fig. 14, we compare our numerical results with the neutron-tagged UPC data from the STAR Collaboration [3]. The STAR experiment uses Mn to denote the emission of one or more neutrons. Here, we present two numerical calculations, one including the corresponding probability to account for the neutron emission effect, and the other without. For this calculation, we adopt the prescription given in Eq. (43) (PAR I) and choose $b_{\min} = 2R_A$. The other parametrization gives similar results. Since the neutron emission probability function for $MnMn$ is biased towards smaller impact parameter b_{\perp} values in UPC, we can see from the result in the previous subsection that q_{\perp} broadening effect is stronger in smaller values of b_{\perp} . Therefore, we observe that including the neutron emission probability shifts the peak of the q_{\perp} distribution to a higher q_{\perp} value. We can find that the calculation combined with the neutron emission probability offers an accurate description of the neutron-tagged UPC experimental data from the STAR Collaboration. This calculation shows that the neutron emission probability is important for describing the experimental data with neutron tagging in the low q_{\perp} regime.

In the right plot of Fig. 14, we present the comparison of the average normalized acoplanarity, $\langle\alpha\rangle$, with the CMS data reported in six neutron multiplicity classes. For this calculation, we utilize both parametrizations for neutron emission probabilities: PAR I with $S = 108 \text{ fm}^2$ in Eq. (43) for lead ions, and PAR II with $S = 303 \text{ fm}^2$. These two prescriptions yield different probabilities of neutron emission scenarios as a function of the impact parameter b_{\perp} . As shown in the figure, these two prescriptions show the right trend and magnitudes comparing to the CMS data. Furthermore, the average acoplanarity value increases as neutron scenarios transition from $0n0n$ to $XnXn$. We observe that the $\langle\alpha\rangle$ depicts a strong dependence on the parameter S in different neutron scenarios, and the average value $\langle\alpha\rangle$ decreases as the parameter S increases. For example, for the $XnXn$, the peak of the neutron emission probability $P_{nn}(b_{\perp})$ shifts towards a smaller impact parameter b_{\perp} as the parameter S decreases. Furthermore, the edges of the two bands are calculated by varying b_{\min} from $2R_A$ to 14 fm in Eq. (48), and we notice that the average value $\langle\alpha\rangle$ decreases as b_{\min} increases. The average values $\langle\alpha\rangle$ are sensitive to the lower limit of integration b_{\min} , especially for high neutron multiplicity classes.

In Fig. 15, we present the comparison of the normalized α distribution with the CMS data for six neutron multiplicity classes. In this calculation, we employ two different parametrizations for the neutron emission probability: PAR I and PAR II, as previously defined. Both prescriptions can provide a good description of the CMS data. Interestingly, the

peak value of the α distribution shifts to larger value from the $0n0n$ class to the $XnXn$ class. In the large α region, we find that these distributions are insensitive to the choice of the parameter S . In summary, our analysis reveals that the neutron emission probability is essential in describing the measurement with the neutron tagging.

c. Enhancements from the Incoherent Contributions in the Large α Region

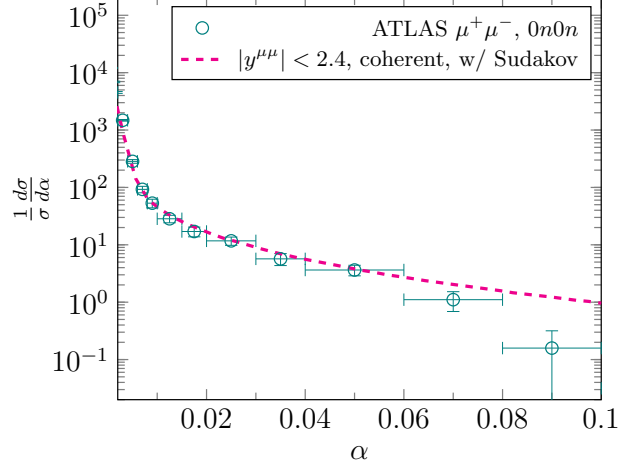


FIG. 16. Comparisons of our result with the ATLAS experimental data [6] in the dimuon pair acoplanarity α distribution for $0n0n$ with the rapidities regions of the dimuon $|y^{\mu\mu}| < 2.4$.

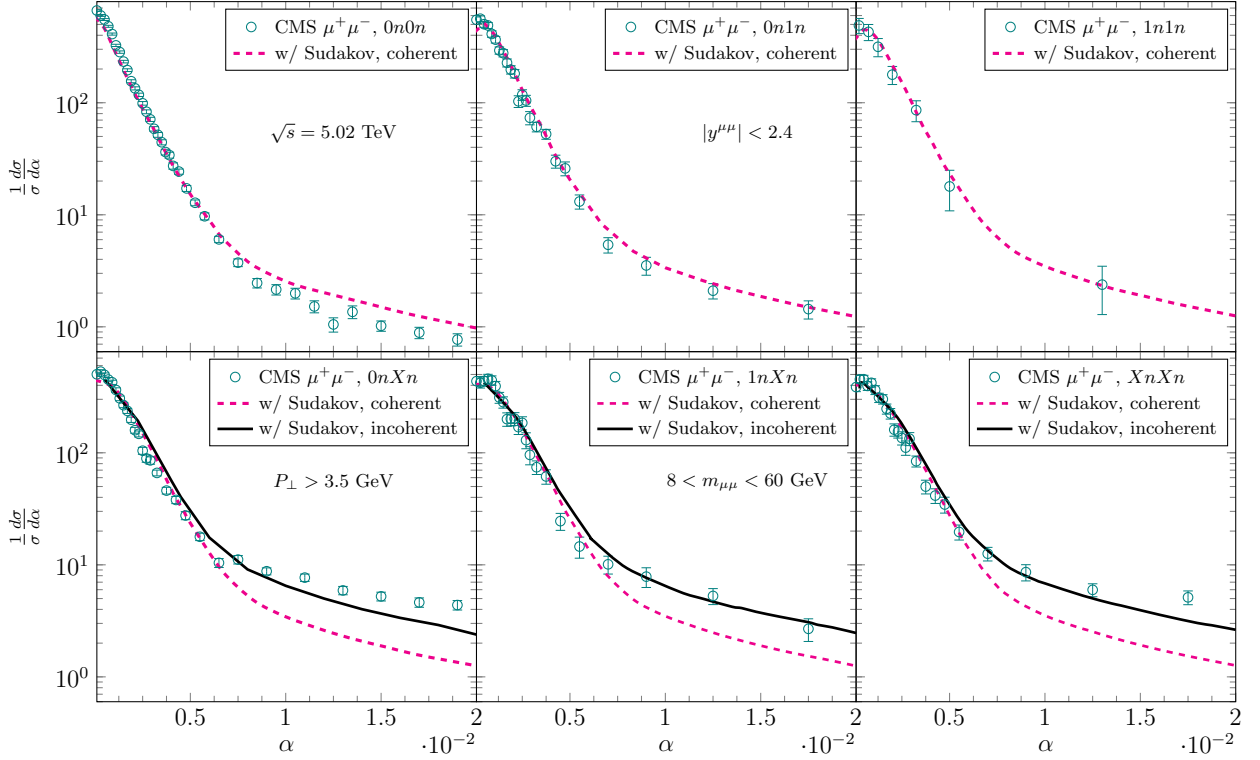


FIG. 17. Comparison of our results with the CMS experimental data [7] in the dimuon pair acoplanarity α distribution with neutron emissions in UPCs.

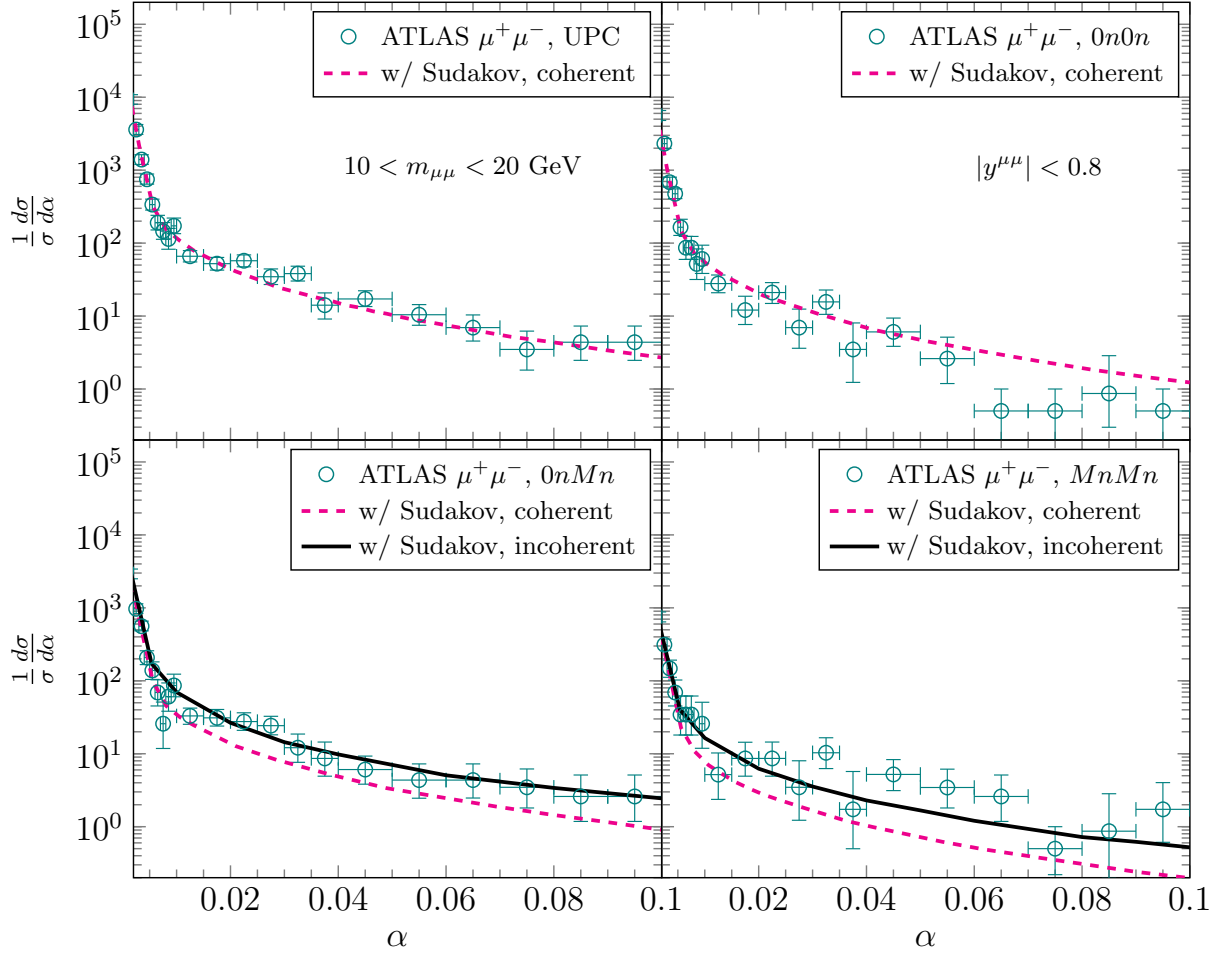


FIG. 18. Comparison of our results with the ATLAS experimental data [6] in the dimuon pair acoplanarity α distribution, taking into account neutron emission in UPCs.

When high transverse momentum photons (i.e., incoherent photons) are emitted from the substructure of a nucleon (proton, neutron), it often leads to the breakup of the emitting nucleus. Using the study on events with neutron emissions in the small α region discussed in the last subsection as calibration, we further incorporate the incoherent contributions into our numerical study and explore the production mechanism of the q_{\perp} broadening effect on the data involving the neutron emission effect in the large α region. As a result, we can demonstrate that the incoherent contributions are indispensable for fully describing the α distribution measurements with neutron emissions.

In the following calculations, since the rest of the observables are not very sensitive to the choice of neutron emission prescription, we will only show numerical results based on Eq. (43), PAR I, as the prescription to account for the neutron emission effect.

Firstly, for the events with one or no neutron emission, the outgoing nucleus is almost intact, and the radiated photons are mostly from the nucleus as a whole. Therefore, the radiation of coherent photons should be the dominant contribution in these events. As shown in the above section, the Sudakov resummation, which resums the final-state soft-photon radiations, is the dominant mechanism for the q_{\perp} broadening in the large α region. In Fig. 16, we show the comparison of our calculations involving the Sudakov effect with the ATLAS $0n0n$ data measured in the rapidities regions $|y^{\mu\mu}| < 2.4$ [6]. We find that the Sudakov calculation can describe the $0n0n$ data from the ATLAS Collaboration in the large α region. In upper panel of Fig. 17, we compare our results incorporating the Sudakov effect with the CMS experimental data [7]. For the three scenarios ($0n0n$, $0n1n$, and $1n1n$), we observe that coherent results incorporating the Sudakov effect accurately describe the CMS data in the large α region. Similarly, as indicated in top panel of Fig. 18 and Fig. 19, the coherent contribution with the Sudakov effect accurately describes both the $0n0n$ and UPC data from ATLAS in dimuon [6] and dielectron [10] pair production process. These results serve as the benchmark for our calculation before including the incoherent contributions.

In addition, the neutron emissions indicate that the disassociation of the nucleus when two colliding nuclei get too

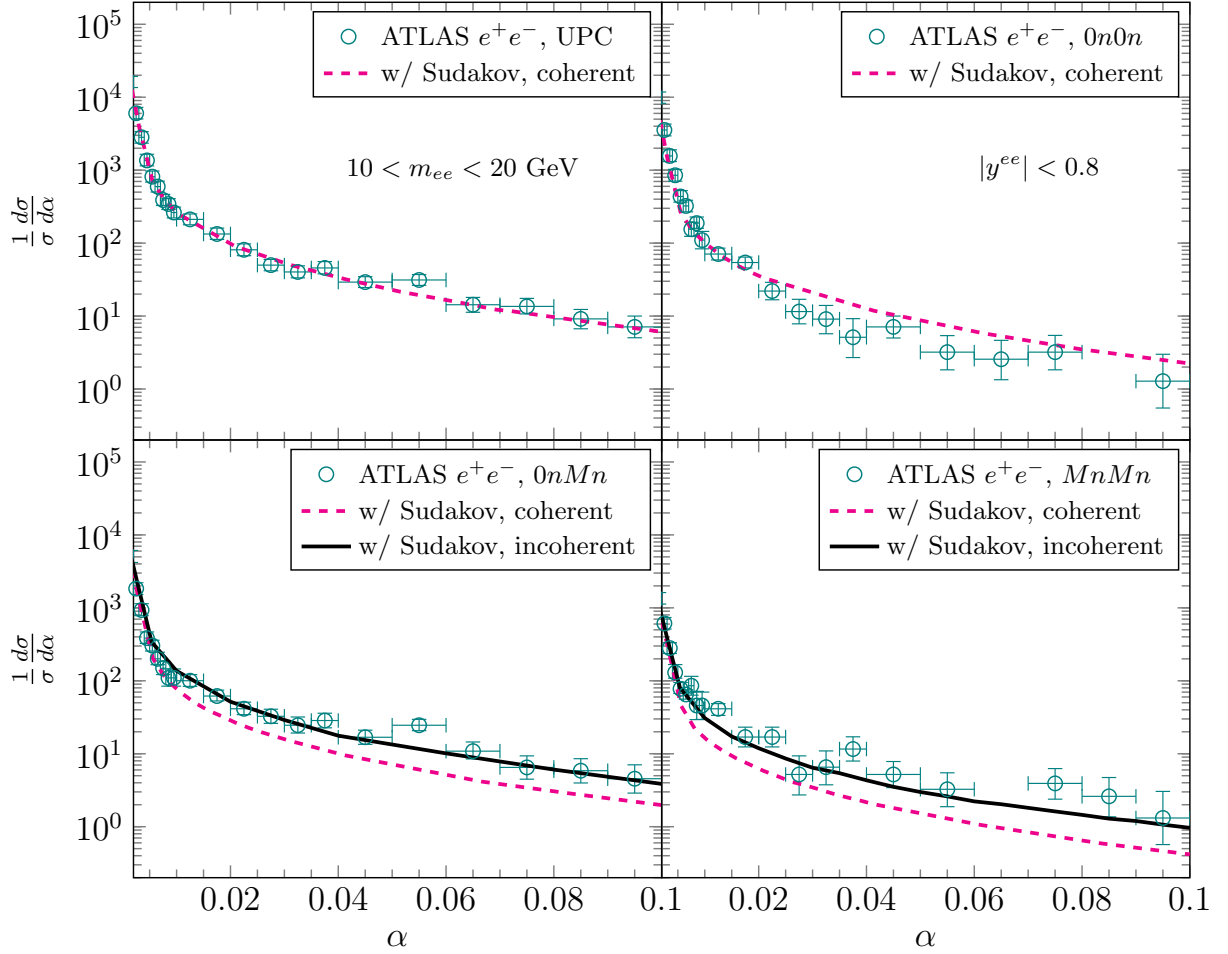


FIG. 19. Comparing of our results with the ATLAS experimental measurements [10] of the e^+e^- pair acoplanarity α distribution with neutron emissions in UPCs.

close to each other in UPCs. In this scenario, the photon might not only be radiated from the nucleus as a whole but also from the protons and quarks inside nucleons. Therefore, the incoherent contribution naturally becomes important for events with more than one neutron emission. Thus, we turn on the incoherent contribution to the photon Wigner distribution. In the lower panel of Fig. 17, we present a comparison between our results with and without the incoherent effect and the CMS data across three scenarios ($0nXn$, $1nXn$ and $XnXn$) in dimuon pair production. Similarly, the low panel of Figs. 18 and 19 illustrate comparisons of our results with ATLAS data in two scenarios ($0nMn$ and $MnMn$) for dielectron and dimuon pair production. The magenta dashed line represents only the coherent contribution with the Sudakov effect, and the black solid line represents the sum of coherent and incoherent contributions with the Sudakov effect. In the small- α region, both curves agree with each other. It shows that, for the event with neutron emissions, the coherent contribution, which stands for the radiated photon from the nucleus as a whole, is still the dominant production mechanism of the q_\perp broadening effect in the small α region. In the large q_\perp region, these coherent calculations with the Sudakov effect underestimate the experimental data for tags with neutron emissions, but the sum of the coherent and incoherent contribution with the Sudakov effect provides good descriptions of the data from CMS and ATLAS Collaborations. It means that besides the Sudakov effect, the incoherent contribution, which represents the radiated photon from protons and quarks, become the dominant contribution to the q_\perp broadening effect in the large α regions for events with multiple neutron emissions.

Let us interpret the numerical results shown in this part. It is evident that the transverse momentum imbalance q_\perp of the lepton pair is small in the small- α region. Thus, the initial heavy nucleus as a unified entity radiates photons with low momenta, and final dileptons do not know the inner structure inside heavy nuclei. In this region, the dominant contribution in the small- α region is from coherent photons. On the contrary, in the large α region where the momentum imbalance of the dilepton pair q_\perp is much larger than $1/R_A$, the coherent contribution to the broadening drops off very rapidly as q_\perp increases. In this case, incoming photons with high transverse momentum

are mostly emitted from the sub-structure in heavy nuclei. Consequently, incoherent photons originating from quarks and protons start to play a vital role.

In the end, through the comprehensive and quantitative comparison with the experimental data above, we demonstrate that the incoherent photon contribution is indispensable for describing the data both with and without neutrons emissions simultaneously.
